

**REMOTE SENSING OF BENTHIC HABITATS IN  
SOUTHWESTERN PUERTO RICO**

By

JEANNETTE ARCE ARCE

Thesis submitted in partial fulfillment for the requirements for the degree of

MASTER IN SCIENCE

In

Geology

UNIVERSITY OF PUERTO RICO  
MAYAGUEZ CAMPUS  
2005

Approved by:

\_\_\_\_\_  
Wilson Ramirez, Ph.D.  
Member, Graduate Committee

\_\_\_\_\_  
Date

\_\_\_\_\_  
Raymond Kokaly M.S.  
Member, Graduate Committee

\_\_\_\_\_  
Date

\_\_\_\_\_  
Fernando Gilbes, Ph.D.  
President, Graduate Committee

\_\_\_\_\_  
Date

\_\_\_\_\_  
Miguel Velez, PhD.  
Representative of Graduate Studies

\_\_\_\_\_  
Date

\_\_\_\_\_  
Johannes Schellekens, Ph.D.  
Department Director

\_\_\_\_\_  
Date

## **Abstract**

Different remote sensing techniques were employed to study benthic habitats in La Parguera, Puerto Rico. These include the comparison of two sensors with different spatial and spectral resolution, IKONOS (1 m, 4 bands) and Hyperion (30 m, 220 bands). Image processing of IKONOS included atmospheric, sun glint, water column corrections, and supervised classifications for the characterization of sea grass, sand and coral. Hyperion data analysis included destriping, atmospheric correction, sun glint correction and classifications. Field data collection was performed by the establishment of three transects with ten quadrants for each habitat class. The best results for image classification in Ikonos imagery were obtained after deglinting of the image with 84 % accuracy and the best result with Hyperion were obtained with the spectral subset in the visible range with an accuracy of 75 %. These results showed that IKONOS had the best results with some limitations on the characterization of the composition of the benthic communities. Hyperspectral shows promise, but the coarse spatial resolution and poor signal to noise of the Hyperion instrument resulted in lower classification accuracy compared to IKONOS.

## **Resumen**

Diferentes técnicas de percepción remota han sido utilizadas para el estudio de hábitat béntico en La Parguera Puerto Rico. Estas incluyen la comparación de dos sensores con diferente resolución espacial y espectral, IKONOS (1 m, 4 bandas) y Hyperion (30 m, 220 bandas). El procesamiento de la imagen de Ikonos incluyó corrección atmosférica, corrección de reflexión especular del oleaje, corrección de columna de agua y clasificaciones supervisadas para la caracterización de yerbas marinas, arenas y coral. El análisis de datos de Hyperion incluyó “destriping”, corrección atmosférica, corrección de reflexión especular del oleaje y clasificaciones. Los mejores resultados para la clasificación de las imágenes de Ikonos se obtuvieron luego la corrección de reflexión especular del oleaje con una precisión de 84% y el mejor resultado con Hyperion se obtuvo de la imagen con las bandas en el rango visible solamente. IKONOS obtuvo mejores resultados con algunas limitaciones en la caracterización de la composición de las comunidades bénticas. Datos hyper espectrales son prometedores pero la resolución espacial grande y la pobre razón de señal versus ruido del instrumento Hyperion resultó en poca precisión al compararse con IKONOS.

## **Acknowledgements**

My sincere thanks to Fernando Gilbes for his advice and guidance. Special thanks to James Goodman for all his support and advice. I also thank committee members Wilson Ramirez and Raymond Kokaly and CenSISS director Miguel Velez for their support. I also gratefully acknowledge Juan Torres, Roy Armstrong, Shirley Morillo, Damaris Torres and Jack Morelock for all their assistance in this project. This work was supported by the Center for, Subsurface Sensing and Imagine Systems, under the Engineering Research Centers Program of the National Science Foundation (CenSISS) Award Number EEC-9986821.

## Table of contents

List of Tables.....	vii
List of Figures.....	viii
Appendixes .....	x
Chapter 1- Introduction	
1.1 Statement of the Problem.....	1
1.2 Objectives .....	3
Chapter 2- Literature Review	
2.1 Remote Sensing.....	5
2.2 Study Site.....	9
Chapter 3- Materials and Methods	
3.1 Image Processing Overview.....	12
3.2 Sensors Characteristics.....	13
3.3 Ikonos Image Processing.....	14
3.3.1 Atmospheric correction.....	15
3.3.2 Masking.....	16
3.3.3 Sun Glint Correction.....	16
3.3.4 Water Column Correction.....	20
3.3.5 Image Classification.....	23
3.4 Hyperion Image Processing	
3.4.1 Atmospheric Correction.....	25
3.4.2 Masking.....	26

3.4.3 Destriping Method.....	27
3.4.4 Sun Glint Correction.....	28
3.4.5 Georeferencing.....	28
3.4.6 Habitat Characterization.....	28
3.5 Fieldwork	
3.5.1 Above Water Measurements.....	30
3.5.2 Bottom Albedo Measurements.....	32
3.5.3 Bottom Types.....	33
3.5.4 Image Validation and Accuracy Assessment .....	34
3.5.5 Expected Benefits .....	37
Chapter 4- Results	
4.1 Image Classifications.....	38
4.2 Ikonos Accuracy Assessment .....	41
4.3 Hyperion Accuracy Assessment.....	43
4.4 Comparison Between Sensors.....	46
Chapter 5- Discussion.....	47
Chapter 6- Conclusions.....	49
Chapter 7-Recommendations.....	51
Chapter 8-References.....	53

### **List of Tables**

Table 1: Characteristics of sensors used in this study.....	13
Table 2: Field validation point data.....	36
Table 3: Overall accuracies, user's and producer's accuracies for IKONOS classifications.....	42
Table 4: Overall accuracies, use's and producer's accuracies for Hyperion classifications.....	45

## List of Figures

Figure 1: NOAA benthic habitat map (map number 158).....	5
Figure 2: Jack Morelock GIS map data subset for study area.....	6
Figure 3: Location of the area of study, southwestern Puerto Rico (Top Left), IKONOS image of Cayo Enrique (Bottom).....	10
Figure 4: IKONOS raw image with the mask (left) and after the sun glint correction (right).....	20
Figure 5: Scatter plot of transformed coral radiance values at different depths in IKONOS image.....	23
Figure 6: Hyperion georeferenced raw data (left), destriped image (center), and atmospherically corrected, destriped and deglinted image (right).....	27
Figure 7: Location of transects at Enrique Reef: A=coral, B=sand, C=sea grass.....	30
Figure 8: Underwater quadrat station for sea grass (left) and bottom albedo measurements with the GER Spectroradiometer in a waterproof cage (right).....	30
Figure 9: Average of above water Remote sensing reflectance measurements for sea grass and sand and coral taken at transects for validation of sensors.....	32
Figure 10: Average of underwater Remote sensing reflectance measurements for sea grass and sand (Left) and coral (Right), taken at transects.....	33
Figure 11: Illustrations representing the different habitat categories used for classification (left- sea grass, center-coral, right-sand).....	34
Figure 12: Field validation point location. A- seagrass and sand, B-seagrass, C-coral, D-sand.....	37
Figure 13: Left, mask applied to Ikonos using a range of values. Right, mask applied to Ikonos using ArcGIS. ....	38
Figure 14: Left, Isodata unsupervised classification. Right, k-means unsupervised classification for Ikonos image.....	39

Figure 15: Minimum distance supervised classifications of IKONOS raw and Deglinted Image. Left, IKONOS raw image classification. Right, IKONOS deglinted image classification.....39

Figure 16: Left, Sea grass red vs. green DII minimum distance classification. Center, Coral red vs green DII minimum distance classification. Right, Sand green vs. Blue DII minimum distance classification.....40

Figure 17: A, Raw minimum distance classified image. B, Hyperion atmospheric corrected and destriped image minimum distance classified image. C, Hyperion atmospheric corrected, destriped and deglinted minimum distance classified image. D, Hyperion spectral subset in the visible region (400-700 nm), georeferenced, destriped and deglinted image.....41

## **Appendixes**

Appendix 1: Sun Glint correction for IKONOS image.....	59
Appendix 2: Water Column Corrections –Lyzenga Method.....	60
Appendix 3: Transect data points.....	68
Appendix 4: Hyperion classifications.....	74

## **Chapter 1**

### **INTRODUCTION**

#### **1.1 Statement of the Problem**

Among the benthic habitats coral reefs are the most important in coastal areas because of their essential role in the marine ecology. They provide nursery for different species and are natural breakwaters. In addition they provide recreational resources for humans. Scleractinean corals are the principal components of modern reefs and are of special interest to scientists since they can provide valuable scientific data on climate change and water chemistry. They are good contributors to the carbonate budget and fossil corals are useful in the determination of geologic history. For example, reef back stepping facilitate the determination of sea level changes through time.

Coral reefs exert control on the surrounding environment. Their contribution to the carbonate budget is important in terms of sediment facies and distribution. Coral reefs are also affected by environmental change. They are sensitive to tectonic activity, sea level changes, variability in temperature, wave energy, salinity, light, and sedimentation.

Mangrove forests are another essential part of marine habitats. These forests contribute to the ecology by providing the right conditions for the development of coral reefs. They act as natural nets controlling sediment input to coastal waters. Their roots are like filters that retain sediments providing low sediment conditions to the coast. They also provide nutrients for certain dinoflagellates (Green, E. et. al., 2000).

The preservation and protection of these benthic habitats is very important due to their environmental role.

Remote sensing provides a tool to study benthic habitats but with certain limitations. New techniques and sensors are constantly produced to facilitate the study of these environments. Coastal remote sensing has disadvantages due to the presence of a water column and its components between the sensor and the target, which affects the reflectance received by the sensor and this has to be considered in the analysis of underwater features. Environmental conditions play an important role in terms of the water properties and the spectral response of the material of interest. Seasonal changes have to be considered since they exert control on the suspended sediments and suspended organic matter.

Modern scientists have considered the use of passive remote sensing techniques for the study of coastal waters because of the sensor's capabilities to map extensive areas. These techniques allow describing benthic features and zones from a satellite or airborne aircraft. Remote sensing techniques can characterize benthic features in the marine ecosystem but require extensive studies.

Multi spectral and hyperspectral sensors have been evaluated in order to study a specific feature or habitat. This research evaluated several sensors for the selection of remote sensing techniques such as band analyses that are useful in the characterization of benthic habitats, including coral reefs.

This study contributes to the efforts in the third and fourth generations of experiments of SeaBED a testbed in coral reefs as part of the Center for Subsurface Sensing and Imaging Systems (CenSSIS). CenSSIS is one of 19 National Science Foundation (NSF) Engineering Research Centers (ERC) in the nation. The center

combines expertise in different areas including the study of coral reefs using remote sensing techniques

The first set of analyses consisted in the study of a coral reef near to the Magueyes Island's Marine Science facility, Cayo Enrique, located at La Parguera in Lajas Puerto Rico. This reef was selected because it is easy to access and has been very well studied.

La Parguera is a coastal region located along the southwest coast of Puerto Rico. Two sensors were tested to characterize sand, sea grass, and coral reefs in the area. These sensors are HYPERION (Hyperspectral Imager) and IKONOS. This study helped to determine which remote sensor and analysis methods were appropriate for coral reef studies and for the characterization of different benthic habitats in the southwest coast of Puerto Rico. These multi-sensor approach and data fusion techniques gave us a better understanding of processes affecting the signal received by the sensors in these regions.

## **1.2 Objectives**

The study of benthic habitats using passive optical remote sensing shows several challenges and requires new approaches and techniques. This study deals with two important questions:

- What is the best combination of spectral and spatial resolution for studying benthic habitats in La Parguera?
- What is the current status of these benthic communities according to the best available remote sensing techniques?

Based on these questions, I have established the following working hypotheses:

- A. High-resolution multispectral imagery will perform better than coarse spatial resolution hyperspectral data.
- B. Different types of benthic habitats can be detected with the techniques developed in this study.

In order to answer these questions and test these hypotheses, the following specific objectives were considered:

1. Combine remote sensing techniques, laboratory analyses and fieldwork to evaluate different sensor resolutions in the study of benthic habitats.
2. The development of better remote sensing techniques for the study of coral reefs and other benthic habitats in Puerto Rico.

## Chapter 2

### LITERATURE REVIEW

#### 2.1 Remote Sensing

In Puerto Rico, the National Oceanic and Atmospheric Administration (NOAA) created a series of GIS maps of the coastal areas. Coral reefs, sea grass beds, mangrove forests and other important habitats were mapped using aerial photography (Kendall et al., 2002). The classification schemes used for benthic maps are based in zones and habitats. The different zones are: shoreline intertidal, lagoon, back reef, reef crest, foreereef, bank shelf, bank shelf escarpment, dredged and unclassified areas. The habitats are: sand, mud, sea grass, sea grass continuous, macro algae, macro algae continuous, macro algae patchy, reef linear reef, reef spur and groove reef, reef patch reef, reef scattered coral rock, reef colonized pavement, reef colonized bedrock, hard bottom reef rubble, hard bottom uncovered pavement, hard bottom uncovered bedrock, land, mangrove, artificial, unknown and no attributes. The different maps of the coast of Puerto Rico are numbered. The map number for the area of La Parguera and Cayo Enrique is 158 and includes all the classifications mentioned before (Figure 1).

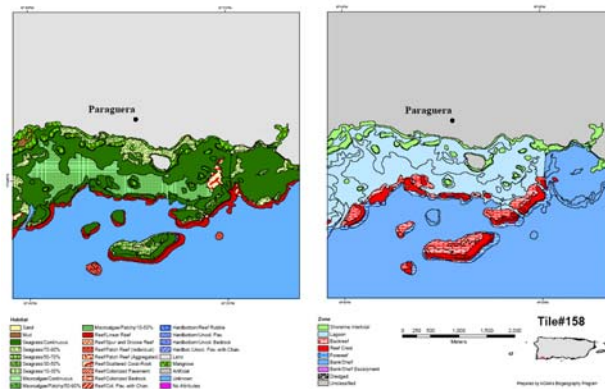


Figure 1: NOAA benthic habitat map (map number 158)

Morelock et al. (1994) created the “Geologic maps of the southwestern Puerto Rico, Parguera to Guanica insular shelf”, which includes a series of detailed geological maps of bathymetry, sediment facies and texture facies, for the area of La Parguera and Guanica insular shelf (Figure 2).

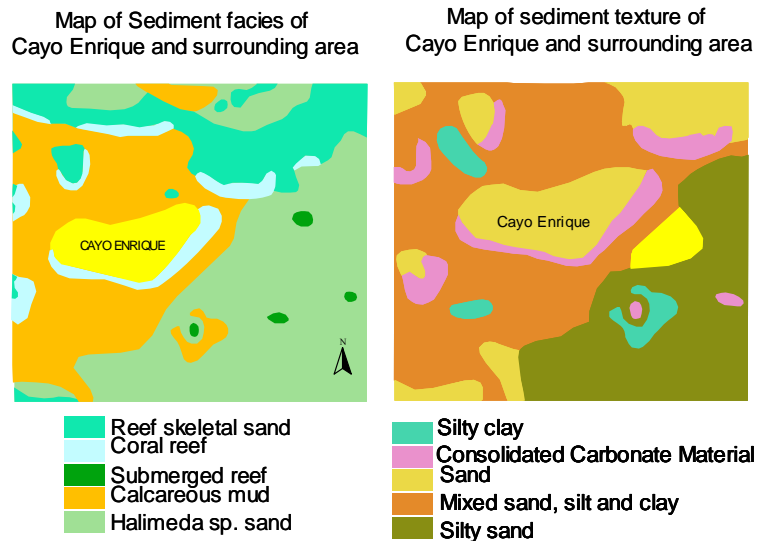


Figure 2: Jack Morelock GIS map data subset for study area.

Remote sensing techniques have been applied to study coral reefs around the world. Due to the current technology limitations the testing of different sensors for benthic habitat studies is of great interest to researchers of different fields. For instance, Mumby et al. (2003) evaluated three optical remote sensing methods for measuring standing crop in the tropical Western Atlantic. They defined empirical relationships of field data with imagery from Landsat Thematic Mapper, SPOT and CASI data to predict standing crop. They also discuss cost benefits and monitoring considerations.

Optical properties of benthic substrates are of great concern when using remote sensing techniques to study benthic habitats. Spectral reflectance of coral species have been analyzed and well studied. Hochberg and Atkinson (2003) collected 247 *in situ*

spectral reflectance of three coral species, five algal species and three sand benthic communities in Kaneohe bay, Oahu in Hawaii. They identified major reflectance features and applied linear discriminant functions to an AAHIS (Advanced Airborne Hyperspectral Imaging System) image.

Holden and LeDrew (2001) took *in situ* reflectance measurements of corals in the U.S. Virgin Islands at various depths over different substratum. They made a comparison between hyperspectral reflectance measured at the top and the bottom of the water column in different water depth. They made a hyperspectral discrimination of healthy versus stressed corals in Fiji Islands, South Pacific and St. Croix, US Virgin Islands, and developed a high spectral resolution library. Hochberg et al. (2003) measured 13,100 *in situ* optical reflectance spectra of 12 reef bottom types in the Atlantic, Pacific and Indian Oceans. They classified fundamental bottom types, processed the spectra and determine spectral separability of bottom types using a classification analysis following the partition method (Rencher, 1995). In their Radiative transfer modeling analysis they determined that corals have a depth of detection limit of 10 to 20 meters in clear waters.

The scientific community is presently evaluating different sensors to study coastal areas. Hochberg and Atkinson (2003) assess the capabilities of seven remote sensors to classify coral, algae and carbonate sand as pure and mixed spectra based on 10,632 reflectance spectra measured *in situ* around the world reefs. They studied the spectral response of two hyperspectral sensors, AAHIS and AVIRIS, and three satellite multispectral sensors, IKONOS, Landsat ETM and SPOT- HRV, and two future satellite narrowband multispectral sensors, PROTO and CRESPO. They conducted discriminant, classification and spectral mixing analysis, and image simulation. Results based on

linearly mixed-sensor specific spectra demonstrate that the hyperspectral and narrowband multispectral sensors discriminate between coral and algae across many levels of mixing, while broadband sensors do not. However narrowband sensors overestimate coral cover. They conclude that it is necessary to design a sensor system specialized to coastal studies. Andre'fouet et al. (2003; unpublished) assessed the potential of IKONOS data for coral reef habitat mapping. Ten IKONOS images of reef habitats around the world were processed, including correction of sea surface roughness and bathymetry, supervised and unsupervised classifications, and accuracy assessment based on ground truth data. The results of IKONOS classification were compared with Landsat 7 data for simple to moderate complexity of reef habitats. Results showed a general linear trend of decreasing accuracy with increasing habitat complexity. In general, IKONOS performed better in accuracy compared to Landsat. The applied sea surface correction (Hochberg et al., 2003) uses the near infrared band to characterize the spatial distribution of relative glint intensity, which is scaled by absolute glint intensity in the visible bands. The result is subtracted from the visible bands filtering out glint effects.

Mumby and Edwards (2002) compared satellite and airborne systems to define habitat categories, supervise image classification, and make an independent assessment of thematic map accuracy. They used CASI, IKONOS, TM, MSS, and HVR data. Mustard et al. (2001) describe an atmospheric correction method applied to a temperate estuary using AVIRIS data. The method is based on scene information only (without *in situ* data) and accounts for non-uniform aerosol scattering glint from water surface and reflected skylight.

Hyperspectral imagery has been considered as a good option for coastal studies because higher spectral resolution provides more information. Goodman and Ustin (2003) employed hyperspectral detector capabilities and image processing tools for mapping and monitoring coral ecosystems in Kaneohe Bay, Hawaii using AVIRIS data. Their analysis starts with at-sensor radiance data, which are then atmospheric and water column corrected, and finally unmixing classified for benthic substrate.

Hyperspectral methods for geologic mapping (Kruse et al., 1997; Kruse et al., 1999; Kruse et al., 2002; Kruse et al., 2003; Kruse, 1996; Kruse and Lefkoff, 1993; Boardman and Kruse, 1993) have been implemented to coastal studies. Kruse et al. (1997) applied techniques developed for geologic mapping to near shore AVIRIS data of the White Point/San Pedro Channel area in California. The processing included data calibration to reflectance, linear transformation to minimize noise and determine data dimensionality, location of the most spectrally pure pixels, extraction of endmember spectra, and spatial mapping of specific endmembers. Kruse (2003) used an end-to-end approach with Hyperion satellite imagery in Buck Island, U.S. Virgin Islands. This methodology included the same standard processing performed to AVIRIS by Kruse et al. (1997).

## **2.2 Study Site**

La Parguera is located in the southwestern coast of Puerto Rico (Figure 3). The Parguera shelf is a bedrock surface composed primarily of karst. This limestone surface has been modified by reef growth and sediment deposition since the last glacial low stand (Morelock et al., 1994). The modern bathymetry and sediment patterns are different from east to west along the Parguera insular shelf. More than 10,000 years ago, when sea level

was lower and the limestone surface of the Parguera shelf was exposed to sub aerial erosion, a karst surface developed (Morelock et al., 1994). The average depth of Parguera shelf is 18 to 20 meters and the shelf width varies from 6 to 10 kilometers. La Parguera shelf was divided by Morelock et al. (1994) in three areas according to wave-energy environments; outer shelf, middle shelf and inner shelf. The outer and middle shelves are 18 to 20 meters deep while the inner shelf is less than 6 m deep. A trace band of reefs separates the inner and middle shelf areas. The middle shelf lies within 4 to 10 meters of the water surface and has more than 15 emergent reefs, which break the surface and hold a reef crest.

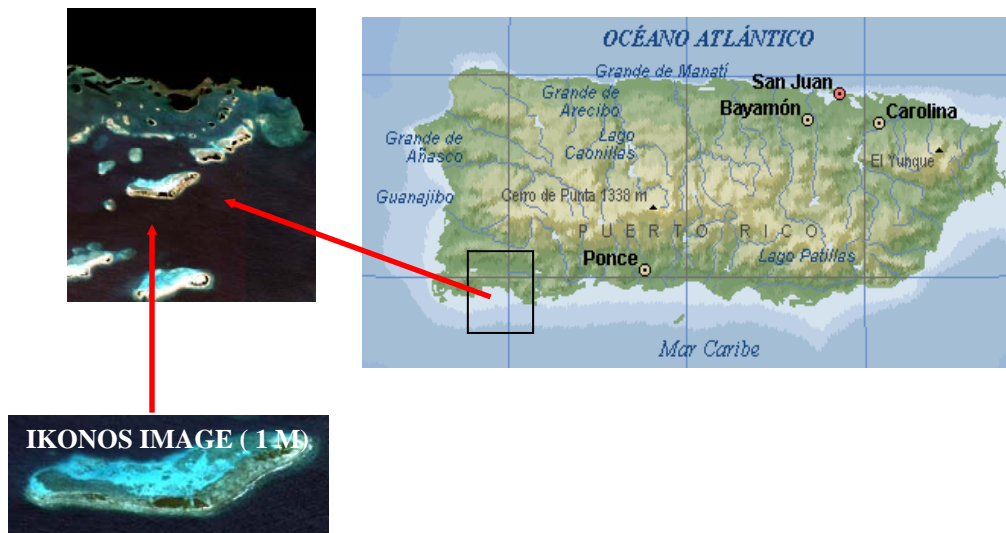


Figure 3: Location of the area of study, southwestern Puerto Rico (Top Left), IKONOS image of Cayo Enrique (Bottom).

The sediment facies in the study area are diverse; reef skeletal sands, calcareous muds, Halimeda species sands, submerged reef and coral reef. Sediments of mixed grain size occur on the middle shelf around Cayo Enrique (Figure 2).

The sediment textures include silty clays and sands, mixed silts, clays and sands, and consolidated carbonate material. The reefs at La Parguera have less than 10 percent terrigenous sediments (Morelock et al., 1994), because no fluvial system approach the sea in the area, local terrigenous runoff is trapped by coastal and near shore mangrove. According to Morelock et al. (1994; 2000) the coral reefs at La Parguera have the highest living coral coverage, diversity and abundance of all southwest Puerto Rico. The reef – building coral taxa, *Montastraea annularis*, *Agaricia agaricites*, *Montastraea cavernosa*, *Porites asteroides*, *Colpophyllia natans*, *Acropora Palmata* and *Acropora cerviconis*, dominate reefs of southwestern Puerto Rico (Morelock et al., 1994;2000). In Cayo Enrique , the forereef is dominated by *Acropora palmata*, until 5 meters. Other species that are abundant at 5 meters in Enrique reef are, *Agaricia agaricites*, *Montastraea cavernosa*, *Montastraea annularis* and *Diploria sp* (Ramirez unpublished MS Thesis, 1992). At 10 meters depth all the species remain except *Agaricia agaricites*. Enrique reef has a slope of 45 degrees and an approximate depth of 25 meters.

## **Chapter 3**

### **MATERIALS AND METHODS**

#### **3.1 Image Processing Overview**

Two images from La Parguera were used in this study. Hyperion, acquired in 2002 and IKONOS acquired in 2000. IKONOS image was georeferenced, and atmospherically and radiometrically corrected using ENVI 4.0 software. A simple dark pixel subtraction method was applied to the image. This is because the image is part of a set of IKONOS images acquired by the government of Puerto Rico to be used as a reference only, without any metadata information. A mask was applied to surface features such as mangroves and land in order to facilitate the classification of the benthic substrate. Sun glint effect was removed from the image using the algorithm described in Hochberg et al. (2003) and called Deglint V1.1. This algorithm uses the near- infrared band to characterize the spatial distribution of relative glint intensity. Then it is scaled by absolute glint intensities in each of the visible bands. A water column correction technique developed by Lyzenga (1981) was applied in order to reduce the effect of the water column, its components and variable depth. This water column correction is an image-based technique that compensates for the effect of variable depth. This method produces a depth invariant bottom index for pairs of spectral bands. Finally supervised and unsupervised classifications were performed for algae, sand, coral, shallow water, and deep water.

Hyperion image processing included destriping, atmospheric correction, removal of glint effects and the creation of a mask. The mask was applied to land, mangrove areas, and waves generated by boats. The image destriping was accomplished using the

method described in Kruse et al. (2003). This method adjusts image column brightness based on a calculated offset relative to average detector response. Atmospheric correction was performed using Atmospheric Correction Now (ACORN 4.0) software. Deglinting of the image was performed by the application of the deglint algorithm *750 Normalizing* developed by Lee et al. (1999). It assumes that the glint correction is constant at all wavelengths and the offset is calculated so that 750 nm reflectance equals a spectral constant,  $\Delta$ . Then values of raw remote sensing reflectance are used to determine an approximation of actual remote sensing reflectance. A spectral subset in the visible range (400-700 nm) were selected in the processed Hyperion image and classified.

### **3.2 Sensors Characteristics**

The characteristics of the sensors used in this study are shown in Table 1.

Table 1: Characteristics of sensors used in this study

Sensor	Bands	Spectral Range	Spatial Resolution	Image area	Sensor technology	Orbit	Inclination
IKONOS	4	0.45-0.90 $\mu$ m	1 m	11 km x 1000 km	Linear array Pushbroom	681 km	----
HYPERION	8-57 79-224	0.4-2.4 $\mu$ m	30 m	7.5 km x 100 km	Pushbroom spectroradiometer	705 km	98.2 <sup>0</sup>

All the images were processed using the ENVI 4.0 software, which is a processing system, designed to provide complete analysis of satellite and aircraft remote sensing data. This software includes tools for spectra extraction, the use of spectral libraries and it analyzes high spectral resolution image datasets.

An essential part of the data analysis process includes the calibration of images to surface reflectance, called the radiometric calibration of the images (Clark et al., <http://speclab.cr.usgs.gov/PAPERS.calibration.tutorial/calibntA.html>). First, the data is atmospherically corrected using radiative transfer algorithms by adjusting atmospheric absorptions in the model and removing the atmospheric effect (Clark et al., <http://speclab.cr.usgs.gov/PAPERS.calibration.tutorial/calibntA.html>). This characterizes and removes the effects of Rayleigh and aerosol scattering in the atmosphere (path radiance) and provides a correction for spectral response relative to wavelength. This correction was done with ENVI 4.0 module called ACORN.

Each distinct image was georeferenced. Pre processing methods were applied to both satellite images and supervised and unsupervised classifications were performed to each image after each processing technique to determine different zones (or classes) based on the spectral response.

### **3.3 IKONOS Image Processing**

The IKONOS image was acquired from the Puerto Rico Department of Transportation (DOT) in 2001. This image does not have metadata because the DOT did not request it. The image map coordinate is in meters, Projection State Plane Nad 83. Digital numbers were converted to units of calibrated radiance ( $\text{Wm}^{-2}\text{sr}^{-1}\text{nm}^{-1}$ ) using the equations provided by official information on the website of Space Imaging (<http://www.spaceimaging.com/>). The image calibration to radiance equation is

$$L_{ij,k} = \text{DN}_{ij,k} / \text{CalCoef}_k \quad (1)$$

Where:

$i,j,k$  = IKONOS image pixel  $i,j$  in spectral band  $k$ ,  $L_{i,j,k}$  = in-band radiance at the sensor aperture ( $\text{mW}/\text{cm}^2 \cdot \text{sr}$ ),  $\text{CalCoef}_k$  = in-Band Radiance Calibration Coefficient ( $\text{DN} \cdot \text{cm}^2 \cdot \text{sr}/\text{mW}$ ),  $\text{DN}_{i,j,k}$  = image product digital value (DN).

Image processing included atmospheric correction using dark pixel subtract, sun glint correction, water column correction, and supervised classifications for the characterization of sea grass, sand and coral.

### ***3.3.1 Atmospheric correction***

A dark pixel subtraction method was applied to the IKONOS image since an atmospheric correction to remove path radiance with ACORN software (version 4.0) was not viable. This is because the image was lacking of metadata. In order to correct the IKONOS image with ACORN we need the specific image date and image average time of collection (day/month/year) available in the metadata file. The dark pixel subtraction method assumes that somewhere in the image is a pixel with zero reflectance, that way the radiance recorded by the sensor is solely attributable to path radiance (Green et.al. 2000). It assumes that scattering is zero in the infrared band but present in the bands with shorter wavelength. Then the minimum pixel value in each band is subtracted from all other pixels to remove path radiance. This method was applied using a feature available in ENVI 4.0.

### ***3.3.2 Masking***

Masking of the IKONOS imagery was performed using ArcGIS software (version 8.0). A mask was intended to apply using ENVI 4.0 with the determination of a range of values. Pixels on sea were masked as well as pixels on land. A geotiff was made for the IKONOS image; polygons were made in ArcGIS covering the surface features including land, mangrove, boats and waves induced by boats. The shapefile was imported as an .evf file and the mask applied in ENVI 4.0.

### ***3.3.3 Sun Glint Correction***

Glint is reflected light on the crests or slopes of waves generated by winds. This effect is a factor in wide field of view acquisition airborne or satellite missions. To remove this effect on the imagery a sun glint correction was performed with the algorithm described in Hochberg et al. (2003) and called Deglint V1.1. This algorithm uses the near- infrared band to characterize the spatial distribution of relative glint intensity assuming that this band exhibits maximum absorption and minimal water leaving radiance over clear waters. Then it is scaled by absolute glint intensities in each of the visible bands. The result is subtracted from the visible bands filtering out glint effects.

Total radiance,  $L_{TOT}(\lambda)$ , is measured at an airborne or spaceborne spectral imaging system with specific angular dependencies corresponding to ground horizontal

spatial positions (x,y). The  $L_{TOT}(\lambda)$  measured by a radiometer pointed downward at sea surface is:

$$L_{TOT}(\lambda) = L_{atm}(\lambda) + T(\lambda) \times L_g(\lambda) + T(\lambda) \times L_w(\lambda) \quad (2)$$

Where  $L_{atm}(\lambda)$  is path radiance generated by scattering in the atmosphere.  $L_g(\lambda)$  is glint radiance generated by specular reflection at the sea surface of direct sunlight and diffuse skylight.  $L_w(\lambda)$  is the water-leaving radiance generated below the sea surface.  $T(\lambda)$  is the atmospheric transmittance.

The spatial distribution function of  $L_{TOT}(\lambda)$  is  $f_{TOT}(x,y)$ , each of the other radiances have their own spatial distribution function. For such image data, (1) is:

$$f_{TOT}(x,y:\lambda) \times L_{TOT}(\lambda) = f_{atm}(x,y:\lambda) \times L_{atm}(\lambda) + T(\lambda) \times f_g(x,y:\lambda) \times L_g(\lambda) + T(\lambda) \times f_w(x,y:\lambda) \times L_w(\lambda) \quad (3)$$

Where  $f_w(x,y)$  is determined by the spatial distribution of subsurface features including the water column and seafloor.  $F_g(x,y)$  is determined by sea state and observation geometry relative to illumination geometry.  $F_x(x,y:\lambda)$  provide relative scaling factors at each (x,y:  $\lambda$ ), and absolute magnitudes are provided by the radiances  $L_x(\lambda)$ . After atmospheric correction (2) becomes:

$$[f_{TOT}(x,y:\lambda) \times L_{TOT}(\lambda)]' = f_g(x,y:\lambda) \times L_g(\lambda) + f_w(x,y:\lambda) \times L_w(\lambda) \quad (4)$$

For subsurface features, the quantity of concern is  $[f_w(x,y:\lambda) \times L_w(\lambda)]$  from the subtraction of  $[f_g(x,y:\lambda) \times L_g(\lambda)]$  from the atmospherically corrected image.  $f_g(x,y:\lambda)$

and  $L_g(\lambda)$  must be estimated for all wavebands to be used in the analysis of subsurface features. Geometrically shallow water is optically deep, at these wavelengths.

$L_w(\lambda)$  tends toward zero and equation (3) is reduced to

$$[f_{TOT}(x,y:NIR) \times L_{TOT}(NIR)] = f_g(x,y:NIR) \times L_g(NIR) \quad (5)$$

It means that after an atmospheric correction a NIR image of an aquatic environment is basically a measure of spatially relative glint intensity.  $f_g(x,y:NIR)$  is weighed by absolute glint intensity  $L_g(NIR)$ . The real index of refraction of the water is nearly equal at visible and NIR wavelengths. Therefore the relative amount of downwelling radiance reflected upward by the water surface is independent of wavelength and only a function of geometry.

$$f_g(x,y:VIS) = f_g(x,y:NIR) = f_g(x,y) \quad (6)$$

This equation means that relative glint intensity  $f_g(x,y)$  is constant across all visible and near infrared wavelengths, even despite the fact that absolute glint intensity varies with wavelength. Absolute magnitude of  $L_g(VIS)$  is determined and scaled to  $f_g(x,y)$  and subtracted from  $[f_{TOT}(x,y:VIS) \times L_{TOT}(VIS)]$  to produce the image of  $[f_w(VIS) \times L_w(VIS)]$ .

The NIR waveband is scaled to determine  $f_g(x,y)$ , where its minimum is zero and its maximum one. The locations of brightest  $(j,i)$  and darkest  $(j',i')$  NIR pixels are determined, which represents the highest and lowest glint values.

This is  $L_g(\text{NIR})+L_w(\text{NIR})$  and  $L_w(\text{NIR})$ , respectively. Where  $L_g(\text{NIR})$  is computed by:

$$\begin{aligned} L_g(\text{NIR}) &= f_g(j,i:\text{NIR}) \times L_g(\text{NIR}) - f_g(j',i':\text{NIR}) \times L_g(\text{NIR}) \\ &= [L_g(\text{NIR}) + L_w(\text{NIR})] - L_w(\text{NIR}) \end{aligned} \quad (7)$$

The NIR image is scaled to the range of zero to one by:

$$f_g(x,y) = \frac{[f_{\text{TOT}}(x,y:\text{NIR}) \times L_{\text{TOT}}(\text{NIR})] - L_w(\text{NIR})}{L_g(\text{NIR})} \quad (8)$$

The maximum absolute glint intensities  $L_g(\text{VIS})$  is determined in each visible waveband, with VIS wavebands substituted for the NIR band.;

$$\begin{aligned} L_g(\text{VIS}) &= f_g(j,i:\text{VIS}) \times L_g(\text{VIS}) - f_g(j',i':\text{VIS}) \times L_g(\text{VIS}) \\ &= [L_g(\text{VIS}) + L_w(\text{VIS})] - L_w(\text{VIS}) \end{aligned} \quad (9)$$

Then the deglinted VIS wavebands are computed by:

$$F_w(x,y:\text{VIS}) \times L_w(\text{VIS}) = [f_{\text{TOT}}(x,y:\text{VIS}) \times L_{\text{TOT}}(\text{VIS})] - f_g(x,y) \times L_g(\text{VIS}) \quad (10)$$

This glint removal technique assumes that  $L_w(\text{NIR})$  is zero for the whole image, but there is always some residual radiance in a NIR image, especially in the absence of an atmospheric correction. Another source of error is the estimation of  $L_g(\text{VIS})$ , the value of  $[f_{\text{TOT}}(x,y:\text{VIS}) \times L_w(\text{VIS})]$  at the brightest pixel  $(j',i')$  is subtracted by the value at

the darkest pixel  $(j',i')$ . The implicit assumption is that  $L_w(\text{VIS})$  is the same for both pixels. The sun glint correction of IKONOS image performed very well and subsurface features were more visible as shown in Figure 4.

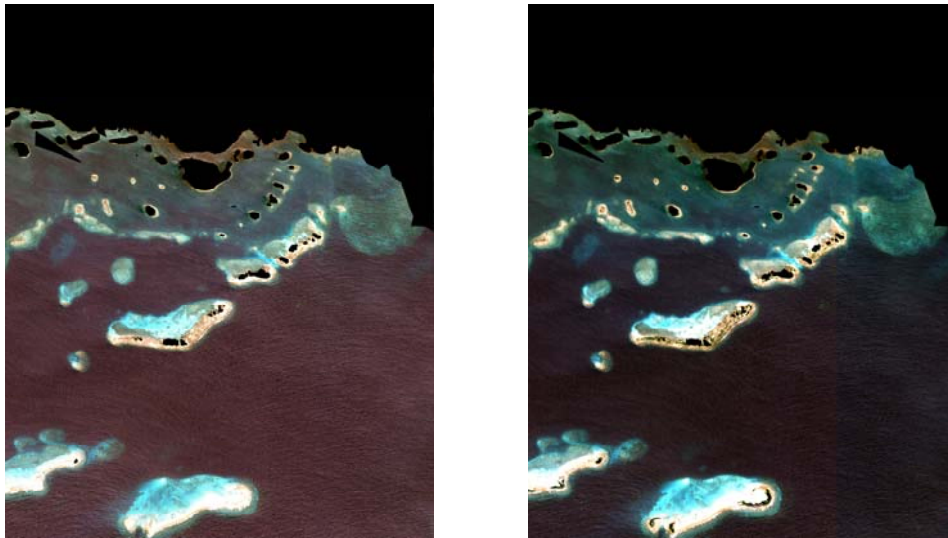


Figure 4: IKONOS raw image with the mask (left) and after the sun glint correction (right).

### ***3.3.4 Water Column Correction***

Attenuation is a process that occurs when light penetrates water and its intensity decreases exponentially with increasing depth and it is wavelength dependent. At the visible range of the spectrum, the red portion attenuates faster than the shorter wavelengths of the blue portion. The decay of light intensity with increasing depth is a consequence of absorption and scattering in the water. Absorption is also wavelength dependent and in coastal waters is caused mostly by suspended materials like algae, organic and inorganic particles, dissolved organic compounds, and by the water itself. Scattering is due to the interaction of suspended particles in the water and increases with the turbidity of the water.

The water column correction technique used in this research is the method developed by Lyzenga (1981). It is an image-based technique to compensate for the effect of variable depth. This method produces a depth invariant bottom index from each pair of spectral bands and is suitable only in areas with good water clarity.

Scattering in the atmosphere and external reflection from the water surface should be removed prior to the water column correction. Previous to this correction the algorithm for sun glint correction was applied, which removed the effect of reflected light on the crests or slopes of waves as well as the atmospheric effect.

In clear waters the intensity of light decays exponentially with increasing depth, consequently radiance values will decrease linearly with increasing depth. In this method values of radiance are transformed using natural logarithms (ln). Then a relationship with depth becomes linear. For data that has been atmospherically corrected the equation is:

$$X_i = \ln(L_i) \tag{11}$$

Where  $X_i$  is the transformed radiance of a pixel in band  $i$ , and  $L_i$  is the pixel radiance in band  $i$ . This is the equation that was used because prior to this water column correction other methods for atmospheric correction and glint correction were applied to the image.

The attenuation coefficient ( $k$ ) describes the severity of light attenuation in water for a spectral band. Pixels of uniform substratum and variable depth are selected; the pixel data in both bands are transferred to a spreadsheet and converted to natural logarithm. The ratio of attenuation coefficients between pairs of spectral bands is calculated from the imagery itself using the pixel information. Two bands are selected

and a bi plot made of log-transformed radiances for the same substratum at different depths (Figure 5). Pixel values for each band will vary linearly according to their depth. The gradient of the bi-plot represents the relative amounts of attenuation in each band and the ratio of attenuation coefficient between bands (K). This ratio is independent of bottom type. The line represents an axis of radiance values for a specific bottom type. The gradient of each line should be identical because the ratio of attenuation coefficients is dependent only of wavelength of the band and clarity of the water. The y intercept for each bottom type is an index of bottom type, independent of depth. Before the implementation of depth invariant index processing all areas of land, mangrove, boats and clouds should be masked. Based on the equation of a straight line:

$$Y=p+q*x \quad (12)$$

Where p is the y intercept, q is the gradient of the regression of y on x. If the equation is rearranged to give the y intercept:

$$P=y - q*x \quad (13)$$

Subsequently, the depth invariant index equation is implemented to the whole image;

$$\text{Depth-invariant index}_{ij} = \ln(L_i) - [(k_i/k_j) * \ln(L_j)] \quad (14)$$

Each pair of spectral bands will produce a single depth invariant band of bottom type. The resulting image is then processed for analysis of the benthic substrate.

Three Depth Invariant Index bands for each substrate resulted from the processing of the data. The bands plotted were; green vs. blue, red vs. blue and red vs. green. (See Appendix A). These index values are not related to radiance or reflectance measurements. The point collection depths for the three bottom types are not equal. The attenuation coefficient of the three bottom types is not the same because the points were not collected at similar depths or similar water conditions. It causes erroneous results and is a limitation of the method.

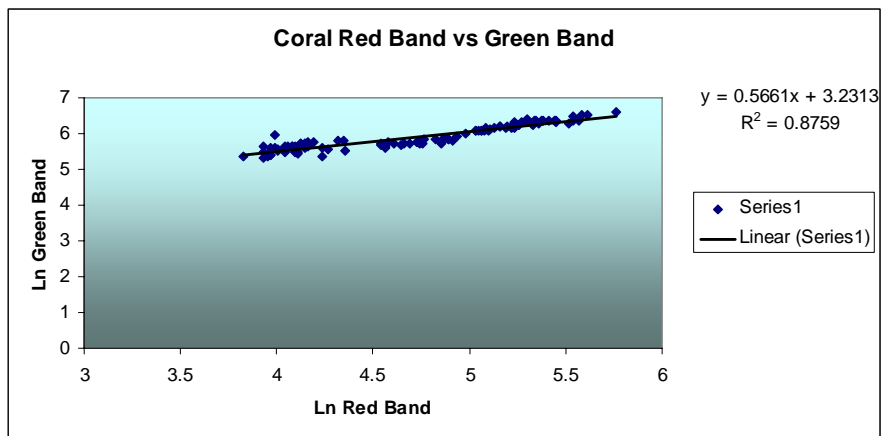


Figure 5: Scatter plot of transformed coral radiance values at different depths in IKONOS image.

### 3.3.5 Image Classification

Band analysis, supervised and unsupervised classifications were conducted for each Depth Invariant Index band to determine different zones (or classes) based on the spectral response. A set of 100 points were selected for each habitat class at different depths.

The areas selected for point collection were: Cayo Media Luna (3.04 m depth), and Cayo Enrique (1.37 m depth) for sand, Laurel (4.57 m depth ) and Mario (0.91 m depth) for coral and Laurel (3.66 m depth) and Cayo Enrique (1.5 m depth) for seagrass. The regions of interest (ROI's) used for classification were; sea grass-red (1751 points), sand- green- (990 points), coral-blue (3034 points), deep water- yellow (4096 points) and shallow water- cyan (4896 points). The Depth Invariant Index bands were classified with each supervised classification method available in ENVI. All the classification methods available in ENVI were tested and the best results were obtained with the minimum distance method. In this method training data is used only to determine class means and classification is performed by placing a pixel in the class of the nearest mean (Richards and Jia, 1999). This method does not use covariance data and it is not as flexible as other classification methods. Given that covariance data is not used in this technique class models are symmetric in the spectral domain (Richards and Jia, 1999). Then elongated classes will not be well modeled. The six classes used for classification were sand, sea grass, coral, deep water, shallow water and the land mask.

### **3.4 HYPERION Image Processing**

Hyperion image was acquired in August 15, 2002. Hyperion data analysis was performed using ENVI hyper spectral processing version 4.0. It includes atmospheric correction, destriping, an application of a Deglint algorithm, Georeferencing using IKONOS as a base image and selection of a spectral subset in the visible range.

### ***3.4.1 Atmospheric Correction***

Atmospheric correction was performed using Atmospheric CORrection Now (ACORN) software (V 4.0) developed by ImSpec LLC, Boulder, Colorado. This is a MODTRAN4 technology that assesses, models and compensates for the atmosphere to allow calibration to surface reflectance without ground measurements. This algorithm was run in processing mode 1, which is a simple atmospheric correction of calibrated hyperspectral data. The parameters used were; tropic atmospheric model, derived water vapor using 940 and 1140 nm bands, and image acorn estimated visibility. Required acorn inputs include; image dimension, image center latitude and longitude, image date and average time, and image acquisition altitude. Acorn values were converted to Remote sensing reflectance dividing reflectance by pi ( $R_{rs} = Ref/\pi$ ).

Other atmospheric correction methods available for Hyperspectral processing are; ATREM, FLAASH and TAFKAA. The ATREM software was developed by the University of Colorado. The ATREM software retrieves scaled surface reflectance from hyperspectral data using a radiative transfer model (Gao and Goetz, 1990).the solar zenith angle is derived from the AVIRIS acquisition time, date, and geographic location and the atmospheric transmittance spectra are derived from seven atmospheric gases. These gases are; methane, carbon dioxide, ozone, nitrous oxide, carbon monoxide, and water vapor. A water vapor “look up” table is created and the water vapor is then estimated for each AVIRIS pixel by determining the band depth and then compares the modeled band depths with the look up table. The resulting product is an image that shows the spatial distribution of diverse water vapor concentrations for each pixel. The result is a

reflectance corrected AVIRIS data and a water vapor image. ATREM version 3.1 was the last release and is not available to any further extent.

FLAASH is an ENVI module for retrieving spectral reflectance from hyperspectral radiance images. It was developed by Spectral Sciences inc. sponsored by the Air Force Phillips Laboratory. It provides an accurate derivation of apparent surface reflectance by derivation of atmospheric properties from Hyperspectral data. Such properties are surface altitude, surface albedo, aerosol and cloud optical depths, water vapor, surface and atmospheric temperatures. It also derives pressure altitude. The radiance spectra is extracted from the HIS data and compared with the MODTRAN “look up” tables pixel by pixel to determine scaled surface reflectance.

TAFKAA is a Hyperspectral atmospheric correction algorithm design to attend the variables in shallow waters. It utilizes look up tables generated with a vector radiative transfer algorithm. Values from these tables are interpolated using information provided in the input files and the spectral characteristics of the input radiance data. The resulting output is optionally in the form of remote sensing reflectance, normalized ground leaving radiance or reflectance (Goodman, 2004).

### ***3.4.2 Masking***

Hyperion processing included the creation of a mask of pixel values from zero to 550. The mask was applied to land and mangrove areas, boats and waves generated by boats (Figure 6).



Figure 6: Hyperion georeferenced raw data (left), destriped image (center), and atmospherically corrected, destriped and deglinted image (right).

### ***3.4.3 Destriping Method***

Striping is caused by sensor system detector imbalance. When a detector fails and goes out of adjustment it provides readings different than the other detectors for the same band (for every pixel  $j$  in a line  $i$ ). The data is valid but have to be corrected to have the same common contrast as the other detectors in the scan. The destriping of Hyperion image was accomplished using the method suggested by Kruse et al. (2003) using Montes code. This method adjusts image column brightness based on a calculated offset relative to average detector response. It assumes that individual detectors are stable and that during data collection cross track detectors covered similar surface materials. In the case of Cayo Enrique the subset selected for the study is mostly covered by coastal waters. An average spectrum is calculated for each of the 256 detectors of Hyperion in a subset and then an overall scene average spectrum is calculated. Every column spectrum is subtracted from the global spectrum to calculate offsets that will be added to each pixel in the corresponding column (Kruse et al., 2003).

### ***3.4.4 Sun Glint Correction***

Deglinting of the image was performed by the application of the algorithm developed by Lee et al. (1999). It assumes that the glint correction is constant at all wavelengths and that the offset is calculated with reflectance at 750 nm equivalent a spectral constant,  $\Delta$  (Lee et. al. in Goodman unpublished Ph.D. thesis).

Therefore, from values of raw Remote Sensing Reflectance,  $R_{rs}^{raw}$  ( $sr^{-1}$ ), an approximation of actual Remote Sensing Reflectance  $R_{rs}(sr^{-1})$  is calculated by:

$$R_{rs}(\lambda) = R_{rs}^{raw}(\lambda) - R_{rs}^{raw}(750) + \Delta \quad (15)$$

$$\Delta = 0.000019 + 0.1(R_{rs}^{raw}(640) - R_{rs}^{raw}(750)) \quad (16)$$

### ***3.4.5 Georeferencing***

An image to image registration of Hyperion was performed in ENVI 4.0 using IKONOS as a base image. The warping method for georeferencing Hyperion was polynomial, degree 1 and the resampling nearest neighbor with background 0.0. Fifty ground control points were selected along the entire subset of La Parguera.

### ***3.4.6 Habitat Characterization***

Supervised and unsupervised classifications were performed in IKONOS and Hyperion images for sea grass, sand, and coral at La Parguera.

All the classifications available in ENVI 4.0 were tested and determined that minimum distance classification bring the best results for this dataset.

A spectral subset of 28 bands in the visible region (400-700 nm) was selected from Hyperion data for classification purposes after all the processing.

Sea grass, algae and possible variations were characterized by visual inspection in the field by scuba diving and in the image. Band ratios and band analysis were performed for the characterization.

Coral reef characterization was performed by inspection in the field and the image, band analysis methods and fieldwork for ground truthing. Supervised and unsupervised classifications will be completed for each image. Possible variations will be considered in the classifications: dead and live coral, and branching versus massive coral.

### **3. 5 Fieldwork**

Fieldwork was performed for accuracy assessment of the image data. Three transects of 20 meter width for each habitat class were initially established at Cayo Enrique (Figure 7). Each transects included ten quadrats of 1 m<sup>2</sup>, separated by a distance of 1 meter. GPS locations and pictures were taken for each quadrat in order to determine the approximated benthic composition. In the case of corals, only the quadrats with large amount of corals (>80%) were considered.

Above water and bottom albedo measurements were taken with the GER 1500 spectroradiometer (Figure 8). The benthic composition and GPS data from transects were used as a reference for the image classifications.

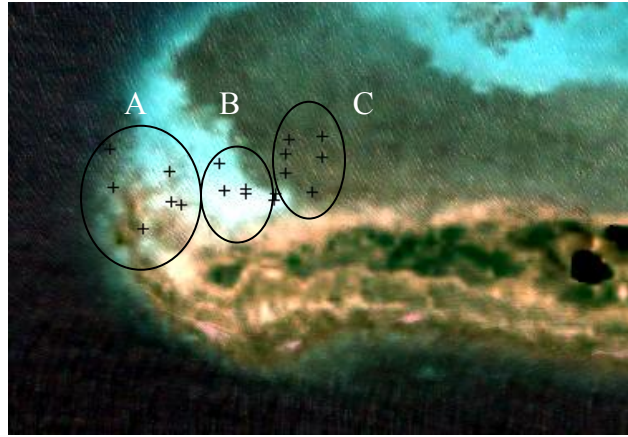


Figure 7: Location of transects at Enrique Reef: A=coral, B=sand, C=sea grass.



Figure 8: Underwater quadrat station for sea grass (left) and bottom albedo measurements with the GER Spectroradiometer in a waterproof cage (right).

### ***3.5.1 Above Water Measurements***

The total signal measured by the remote sensor has a series of components, which must be separated. The atmosphere and the water column are two main components that have to be understood in order to obtain a correct bottom signal. In this research I evaluated the effects of the water column in the Remote sensing Reflectance ( $R_{rs}$ ).

Apparent optical properties depend of the medium and the geometric structure of the light field in the environment (Holden and Le Drew, 2001).  $R_{rs}$  is an apparent optical property controlled by the absorption and the scattering properties of the constituents in the water column, the bottom reflectance, and bottom depth (Lee et al., 2001).  $R_{rs}$  determinations provide a link between imagery from satellite sensors and *in situ* concentrations of optically active constituents, for example, chlorophyll, dissolved organic matter, and particles in the water column (Toole et al., 2000).

Remote sensing reflectance was determined as the ratio of the water leaving upwelling radiance  $L_0$  to incident downwelling irradiance  $E_d$  just above the water surface. The equation used was:

$$R_{rs} = (L_0 - fL_s) / E_d \quad (17)$$

Where  $L_0$  is the total radiance (from the ocean), which is contaminated by the sky radiance ( $L_s$ ) and reflected off the sea surface and it is subtracted in order to obtain the water leaving radiance (Toole et al., 2000).  $E_d$  is the incident downwelling radiance.  $f$  is the Fresnel number which is the reflectance of the sea surface at a viewing angle, which counts for the percent of radiation of the sky that is reflected back to the sensor. At an angle of 45 degrees the Fresnel number is 0.028. Above water measurements as well as the remote sensing reflectance are both sensitive to the proper removal of reflected sky radiance (Toole et al., 2000).

$R_{rs}$  measurements were made with the GER-1500 Spectroradiometer at 45 degrees during clear skies. A clear sky is necessary because above water reflectance measurements vary with cloud conditions.

The GER-1500 Spectroradiometer is an instrument from the Geophysical and Environmental Research Corporation. It is a lightweight, single beam field spectrometer that has a spectral range from 0.3 to 1.1  $\mu\text{m}$  with a spectral sampling of 1.5. The instrument acquires single spectra in milliseconds. Figure 9 shows Remote sensing reflectance measurements taken at transects for validation of sensors. Measurements for sea grass were taken in Cayo Enrique and Media Luna, sand in Cayo Enrique and Media Luna, and coral in Cayo Enrique.

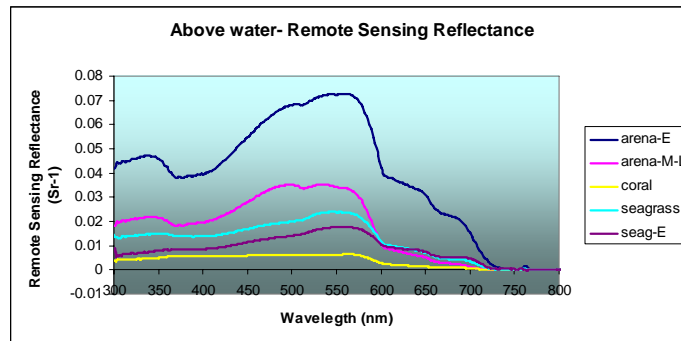


Figure 9: Average of above water Remote sensing reflectance measurements for sea grass and sand and coral taken at transects for validation of sensors.

### ***3.5.2 Bottom Albedo measurements***

The bottom albedo measurements were also taken with the GER 1500 Spectroradiometer in a waterproof cage (Figure 10). A reference spectrum was collected from a calibrated panel (Spectralon) that reflects 99% of the incident radiation. Bottom

albedo was computed based on the ratio of target radiance and reference radiance. The decimal 0.99 refers to the percent reflected by the Spectralon reference.

$$\% \text{ Reflectance} = \frac{\text{Target } \lambda}{\text{Reference Panel } \lambda} * 0.99 \quad (18)$$

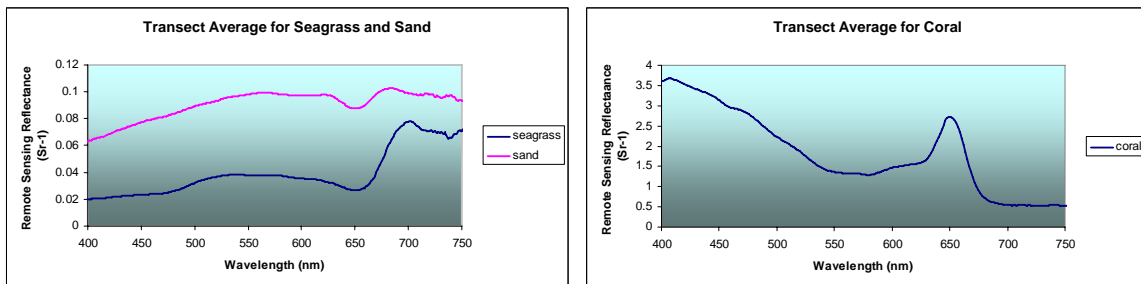


Figure 10: Average of underwater Remote sensing reflectance measurements for sea grass and sand (Left) and coral (Right), taken at transects.

### 3.5.3 Bottom Types

Three bottom types were studied and selected for image classification; sea grass, sand and coral (Figure 11). The percentage of living coral, coral cover or sub categories was not considered for image classification. Although shallow waters and deep waters were considered for classification, bathymetry corrections were not performed to the images. Of the methods applied the Lyzenga method was the only that compensates for variable depth.



Figure 11: Illustrations representing the different habitat categories used for classification( left-sea grass, center-coral, right-sand).

#### ***3.5.4 Image Validation and Accuracy Assessment***

Field validation was conducted by selecting random points for each habitat class along the entire area of study at La Parguera.

Thirty three points (Figure 12) were selected as reference for each habitat class at different locations including the area of Cayo Enrique, the test bed of this study. GPS points and GER Spectroradiometer above water measurements were also taken for the validation of the image data. The thirty two points selected per class were chosen collectively in different regions of the study area and were the same for both images, Ikonos and Hyperion (Figure 12 and Table 2). These points were randomly selected and at the same latitude and longitude in both images. For future studies more points should be collected and must be collected distant from each other and in different areas along the entire area of study. The pixel size in Hyperion (30 m) and the pixel size of Ikonos (1m) produce bias in the accuracy results because the pixel coverage ratio is 1:30 and the coverage of one meter is not exactly the coverage of 30 m, especially in terms of benthic habitats which are variable in composition. The pixel size and distance between points should be considered for point collection.

The accuracy assessment of classified habitat maps was evaluated using the confusion matrix (ENVI 4.0 tutorial). This is calculated by the comparison of the location and class of each ground truth point with the corresponding location and class in the classified image. This error matrix is a square array of rows and columns where the columns represent the reference data and the rows the classification generated by the remote sensed data and each cell has the sampling sited per class. Classified habitat maps were evaluated using the overall, user, and producer accuracy computed from the derived confusion matrices (Green et.al.2000). The overall accuracy is calculated by the sum of the number of pixels classified correctly divided by the sum of all the pixels in the entire ground truth classes. Ground truth ROI's defines the true class of the pixels. The user's accuracy is map based accuracy where the number of pixels correctly classified as a class is divided by the total number of pixels classified in that class. It is the probability that a pixel classified on the image is correctly classified when compared in the field. Error of commission occur when a pixel in a class is included when should be excluded. The producer accuracy is a reference based accuracy based in the probability that the classifier has labeled an image pixel into a specific class given that the ground truth is that class. It is the probability that any pixel in that category has been correctly classified. Correctly classified pixels are divided by the total number of ground reference pixels in that class. Error of omission will be to exclude a pixel that should be included in the class. The producer's and user's accuracy show the classification accuracy of individual classes.

The kappa coefficient is another method for accuracy assessment and is included in the results. The Kappa coefficient is a measure of the proportional improvement by the

classifier over a purely random assignment of classes. It is calculated by multiplying the total number of pixels in all the ground truth classes by the sum of the confusion matrix diagonals, subtracting the sum of the ground truth pixels in a class times the sum of the classified pixels in that class summed over all classes, and dividing by the total number of pixels squared minus the sum of the ground truth pixels in that class times the sum of the classified pixels in that class summed over all classes (ENVI 4.0 Tutorials).

Table 2: Field validation point data associated with figure 12.

<b>SUBSTRATE</b>	<b>DEPTH</b>	<b>LOCATION</b>
<b>Sand</b>	6-7 Feet	Media Luna
<b>Coral Community</b>	2 Feet	Between Media Luna and Laurel
<b>Sea grass</b>	4 ½ Feet	Laurel
<b>Sand</b>	2 Feet	Enrique
<b>Sea grass</b>	2 Feet	Enrique

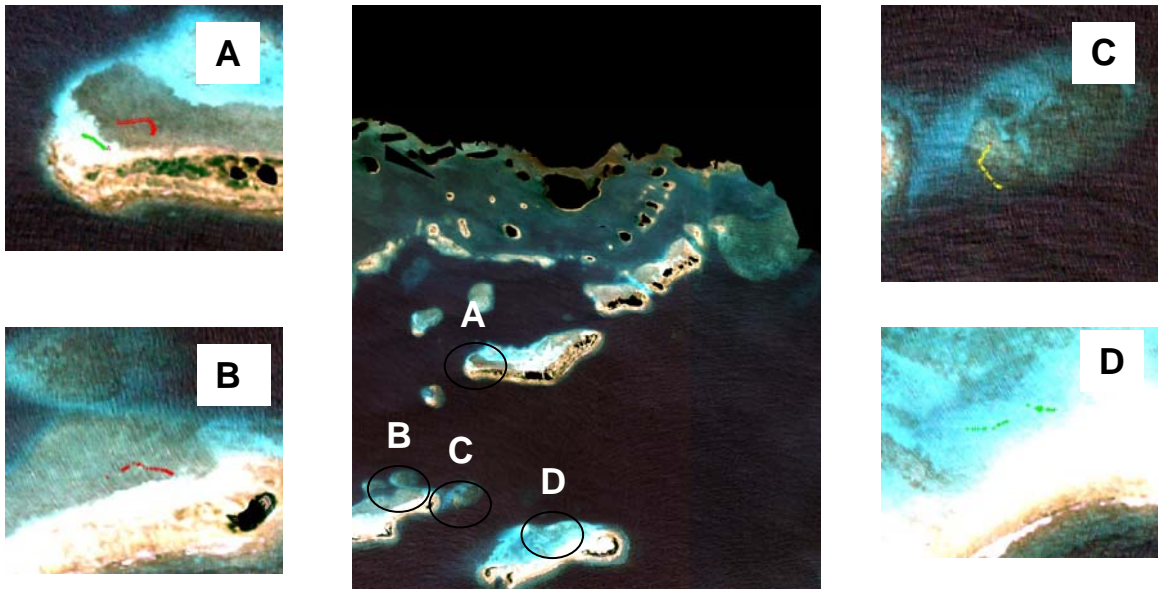


Figure 12: Field validation point location. A- seagrass (Cayo Enrique) and sand, B- seagrass (Laurel), C-coral (Laurel), D-sand (Media Luna).

### ***3.5.5 Expected benefits***

This research provides the baseline for future habitat studies at la Parguera and for the testing of other sensors in this region. Sensors like AVIRIS, LASH and QuickBird are some examples of systems developed for earth studies that can be tested in this area. Field data collected for this project has been already used by engineering students in the testing and development of new image processing techniques and algorithms. The data and results included in this research can assist in the selection of the appropriate sensor and techniques to study benthic habitats at la Parguera. In general these studies are a reference for engineers in the development of sensors and image processing techniques and algorithms. For scientists it is of importance in the selection of cost and time effective sensors and selection of processing techniques. This research is another example of the need to develop a sensor with the qualifications to study underwater features.

## Chapter 4

### RESULTS

#### 4.1 Image classifications

In order to obtain better results in the classification of underwater features masks were applied to the images using a range of values. Different ranges of values were used to create the masks but not all land and mangrove areas were completely covered and underwater pixels were included in the mask (Figure 13). Mask polygons were created using ArcGIS to cover the land areas, mangrove areas well as boats and the waves generated by the boats.

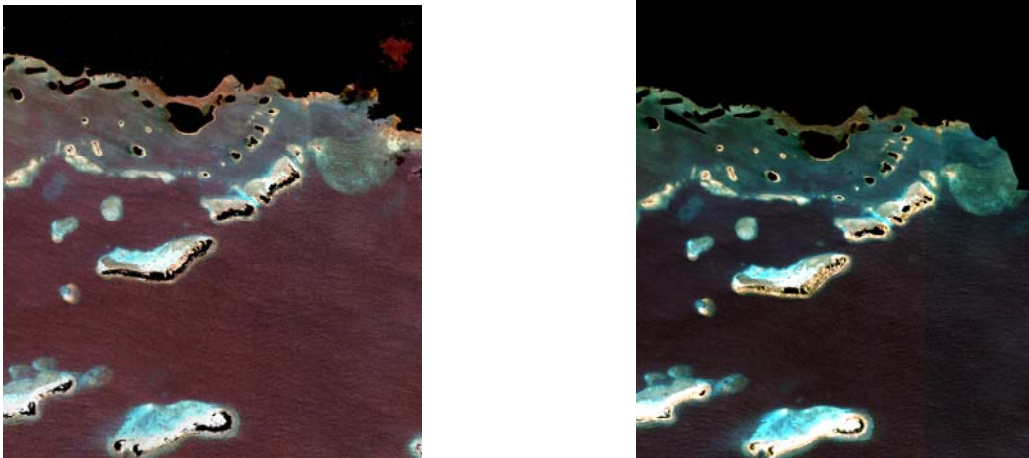


Figure 13: Left, mask applied to Ikonos using a range of values. Right, mask applied to Ikonos using ArcGIS.

All the image classifications available in ENVI 4.0 were applied to the images, including the unsupervised classifications. Unsupervised classifications resulted in inaccurate results and were not considered for mapping (Figure 14). The benthic regions were not clearly delineated. In general the best results were obtained using minimum distance supervised classification. In the case of Ikonos, the best results using minimum distance

classification were obtained after deglinting of the image where the boundaries between different bottom types are enhanced (Figure 13).

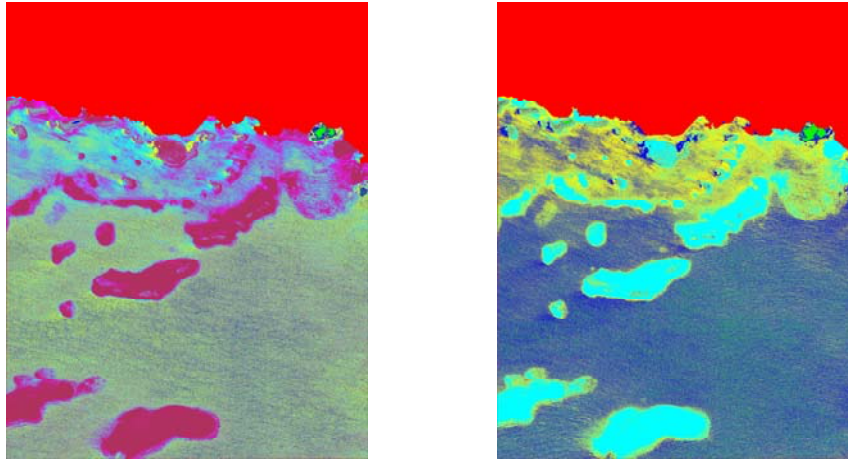


Figure 14: Left, Isodata unsupervised classification. Right, k-means unsupervised classification for Ikonos image.

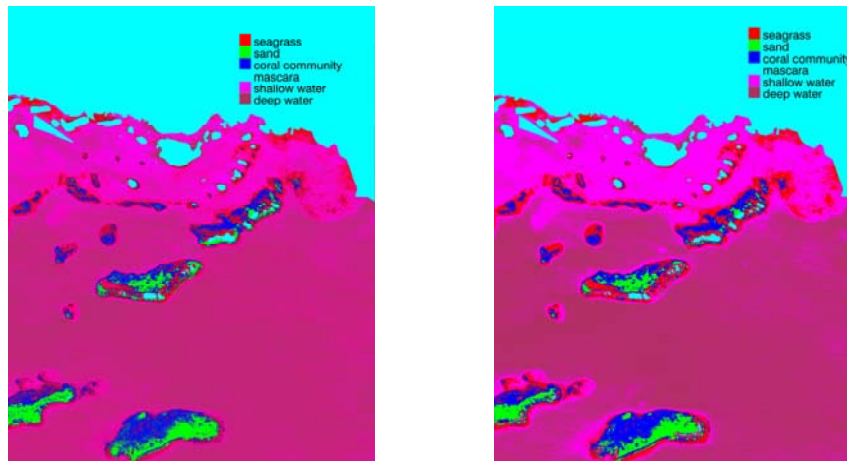


Figure 15: Minimum distance supervised classifications of IKONOS raw and Deglintered Image. Left, IKONOS raw image classification. Right, IKONOS deglintered image classification.

After water column correction the classifications did not improve the results obtained after deglinting (Figure 16). For sea grass the best classification were for bands red vs. green DII minimum distance classification. For coral, the best results were obtained with the red vs green DII minimum distance classification and for sands the green vs. Blue DII minimum distance classification (Figure 14). The classifications performed to other pairs of bands were not accurate when classifying the benthic habitats at La Parguera. In general a specific pair of bands did not perform better than others. For each benthic class a specific pair of bands performed well but did not improve the results obtained before the application of water column correction to Ikonos.

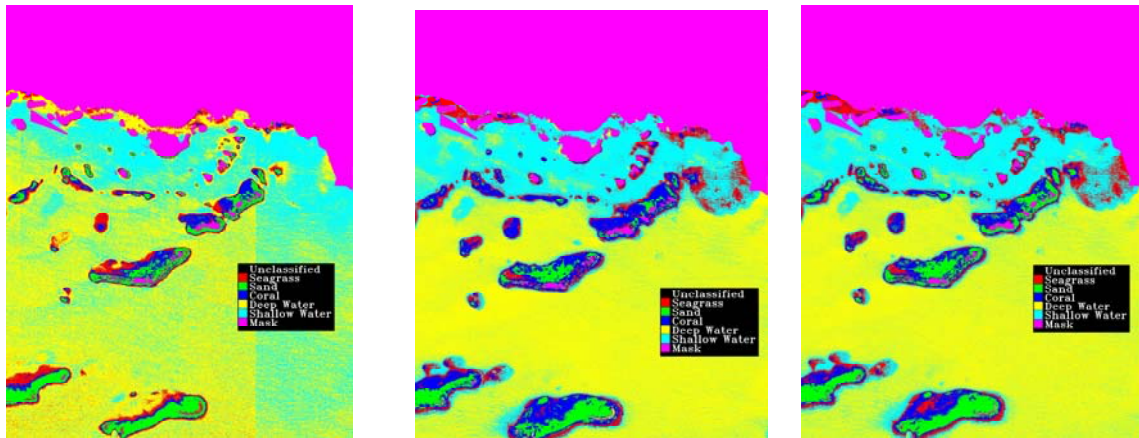


Figure 16: Left, Sea grass red vs. green DII minimum distance classification. Center, Coral red vs green DII minimum distance classification. Right, Sand green vs. Blue DII minimum distance classification.

The supervised classifications of Hyperion were performed after georeferencing of the images. The best results obtained in Hyperion classification were obtained after selecting a spectral subset in the visible bands (Figure 17). After processing, the maps are inaccurate and confusing and the benthic areas are not visible or clearly delineated. With the selection of the spectral subset better results are obtained in the image results.

The low signal to noise ratio of Hyperion and the pixel size and the nature of the post processing are factors that contribute to the results in the whole dataset. The classifications were executed after georeferencing of the images; it may alter the data results after image processing. Errors and original data modification can occur during processing.

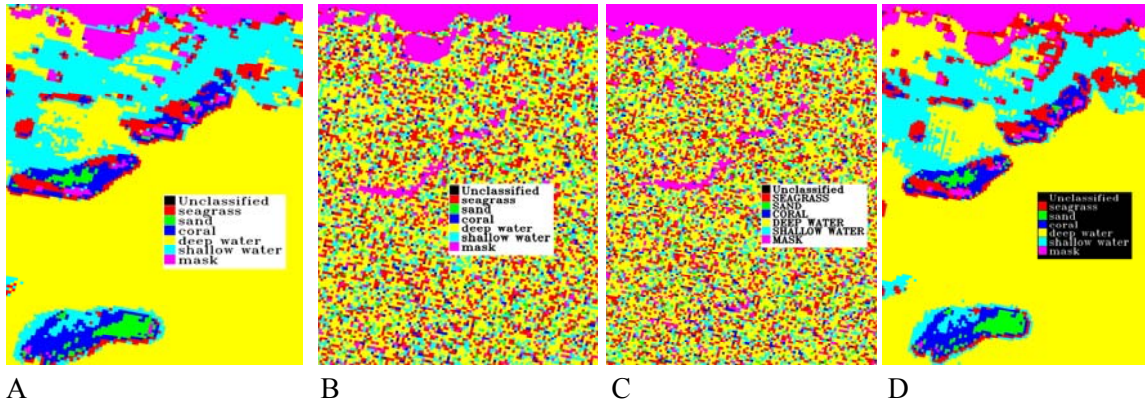


Figure 17: A, Raw minimum distance classified image. B, Hyperion atmospheric corrected and destriped image minimum distance classified image. C, Hyperion atmospheric corrected, destriped and deglinted minimum distance classified image. D, Hyperion spectral subset in the visible region (400-700 nm), georeferenced, destriped and deglinted image.

### **IKONOS Accuracy Assessment**

The deglint algorithm applied to the IKONOS image improved significantly the contrast between subsurface features and boundaries between sand and seagrass areas. Overall accuracy in IKONOS (84.34%) showed significant improvement after deglinting of the image of 13.13 % over the raw image accuracy (71.21%). The improvement was also visible in the user accuracy (probability of a pixel to be classified as the class in the field) after glint corrections; seagrass (66%), sand (100%), and coral (100%) show improvements in this accuracies after correction. Coral shows 28% user accuracy in the raw data and after the glint correction it shows 100% user accuracy, this is a noticeable

improvement in the map classification. Sand (100%) and sea grass (66%) areas also show improvement after deglint corrections. These areas are generally shallow and mostly homogeneous in la Parguera.

No significant improvement was shown after application of the Lyzenga method where the highest overall accuracy were approximately 68% for the depth invariant index band classification of coral, sea grass, and sand. But overall accuracy of these bands was mostly above 50%. The Lyzenga method compensates for variable depth, but no improvement in map accuracy were observed. Also the depths for point collection are variables depending on the substrate. The overall accuracies were below the accuracies obtained in the raw image. The Lyzenga depth invariant index method gave a user's accuracy very low for coral (<26%). The limitation of this method is that the same bottom type may not occur at variable range of depths thus affecting the estimation of diffuse attenuation coefficient (Maritorena, 1996).

Table 3: Overall accuracies, user's and producer's accuracies for IKONOS classifications.

Image	Classification Class	Producer accuracy	User accuracy	Overall accuracy	Kappa Coefficient
<b>IKONOS Raw Image</b>	Sea grass	45.45	45.45	71.21	0.6545
	Coral	24.24	28.57		
	Sand	100.00	97.06		
	Deep Water	84.85	84.85		
	Shallow Water	72.73	64.86		
	Mask	100.00	100.00		
<b>IKONOS Deglinted</b>	Sea grass	100.00	66.00	84.34	0.8121
	Coral	15.15	100.00		
	Sand	100.00	100.00		
	Deep Water	90.91	100.00		
	Shallow Water	100.00	70.21		
	Mask	100.00	100.00		
<b>Lyzenga Coral Green-Blue</b>	Sea grass	6.06	12.50	68.18	0.6182
	Coral	15.15	13.89		
	Sand	100.00	100.00		
	Deep Water	93.94	93.94		
	Shallow Water	93.94	65.96		
	Mask	100.00	100.00		

<b>Lyzenga Coral Red -Blue</b>	Sea grass	57.58	26.03	47.97	0.3758
	Coral	6.06	13.33		
	Sand	100.00	97.06		
	Deep Water	24.24	44.44		
	Shallow Water	100.00	56.90		
	Mask	0	0		
<b>Lyzenga Coral Red-Green</b>	Sea grass	63.64	51.22	67.68	0.6121
	Coral	3.03	8.33		
	Sand	100.00	97.06		
	Deep Water	39.39	52.00		
	Shallow	100.00	62.26		
	Mask	100.00	100.00		
<b>Lyzenga Sand Green -blue</b>	Sea grass	6.06	11.11	68.6486	0.6121
	Coral	15.15	13.89		
	Sand	100.00	100.00		
	Deep Water	93.94	91.18		
	Shallow Water	90.91	68.18		
	Mask	100.00	100.00		
<b>Lyzenga Sand Red - Blue</b>	Sea grass	72.73	57.14	52.53	0.4303
	Coral	3.03	6.67		
	Sand	81.82	96.43		
	Deep Water	48.48	53.33		
	Shallow Water	9.09	23.08		
	Mask	100.00	47.14		
<b>Lyzenga sand Red -green</b>	Sea grass	9.09	17.65	55.05	0.4606
	Coral	3.03	6.67		
	Sand	27.27	90.00		
	Deep Water	90.91	35.71		
	Shallow Water	100.00	100.00		
	Mask	100.00	84.62		
<b>Lyzenga sea grass Green-Blue</b>	Sea grass	6.06	11.11	67.68	0.6121
	Coral	15.15	13.89		
	Sand	100.00	100.00		
	Deep Water	93.94	91.18		
	Shallow Water	90.91	68.18		
	Mask	100.00	100.00		
<b>Lyzenga sea grass Red -blue</b>	Sea grass	62.07	48.65	65.9459	0.5818
	Coral	6.45	16.67		
	Sand	100.00	96.97		
	Deep Water	25.81	44.44		
	Shallow Water	100.00	57.41		
	Mask	100.00	100.00		
<b>Lyzenga Sea grass Red -Green</b>	Sea grass	68.97	60.61	72.22	0.6667
	Coral	3.03	8.33		
	Sand	96.97	96.97		
	Deep Water	66.67	55.00		
	Shallow Water	100.00	75.00		
	Mask	100.00	100.00		

### **4.3 HYPERION Accuracy Assessment**

The overall accuracy for Hyperion did not show improvement after application of the atmospheric correction and the deglint algorithm. Surprisingly the classification that performed the best was the one applied to the raw image data (72.73%). A spectral subset of hyperion were selected after application of the processing methods. Only the bands in the visible range were selected after the processing methods applied and the overall accuracy of the classification results improved slightly from a 72% overall accuracy to a 75% overall accuracy. In this classification the user and producer accuracy of coral class is 0% and producer accuracies of sea grass, deep water and shallow water are 100 %. User accuracies for deep and shallow waters are 89.19 %, for sand 100% and for sea grass 56.9 %. The higher overall accuracy for Hyperion was obtained in the image with the visible bands spectral subset (75.25%). The longer wavelengths of Hyperion have low signal to noise ratio. Selecting only the visible range removes the longer wavelengths in the processing and selects the bands with better signal to noise ratio. This shows that the methods and algorithms applied to the image processing were proficient for some benthic habitats at these levels of processing. The longer wavelengths are used by ACORN in the atmospheric correction this affects the shorter bands in the processing. When the classification is applied to the whole set of bands the results are not as expected. Hyperion image raw data accuracy where similar to the IKONOS raw image accuracy, this shows that the post processing is crucial in order to improve the classifications results.

After application of the atmospheric correction to the unprocessed image the overall accuracy was reduced to 42.93% and after application of the deglint algorithm to that atmospherically corrected image a minimum improvement was observed getting an overall accuracy of 57.07%, but still it did not exceed the overall accuracy obtained in the image with the 400-700 nm spectral subset. Seagrass classification showed 100% in user's and producer's accuracies with the raw image and around 60% after other processing methods. Areas with coral in Hyperion raw data shows 57.14% user accuracy and 72.73% producer accuracy, higher than in the processed images where the accuracy was zero after application of the processing methods. Sand areas show similar results in the user's accuracy with 100% in the raw image and the deglinted image, but lower percentages were observed in producer's accuracy results.

Table 4: Overall accuracies, use's and producer's accuracies for Hyperion classifications.

Image	Classification class	Producer accuracy	User accuracy	Overall accuracy	Kappa coefficient
<b>Hyperion Raw image</b>	Sea grass	100.00	100.00	72.72	0.6727
	Coral	72.73	57.14		
	Sand	45.45	100.00		
	Deep Water	100.00	55.00		
	Shallow Water	18.18	40.00		
	Mask	100.00	100.00		
<b>Hyperion Acorn Corrected</b>	Sea grass	87.88	63.04	49.92	0.3152
	Coral	0.00	0.00		
	Sand	69.70	62.16		
	Deep Water	0.00	0.00		
	Shallow Water	0.00	0.00		
	Mask	100.00	100.00		
<b>Hyperion Acorn Destriped Deglinted</b>	Sea grass	100.00	60.00	57.07	0.4848
	Coral	0.00	0.00		
	Sand	66.67	100.00		
	Deep Water	75.76	29.41		
	Shallow Water	0.00	0.00		
	Mask	100.00	97.06		
<b>Hyperion Acorn Destriped Deglinted-400-700 nm</b>	Sea grass	100	56.90	75.25	0.7030
	Coral	0	0		
	Sand	51.52	100		
	Deep Water	100	89.19		
	Shallow Water	100	89.19		
	Mask	100	100		

### ***4.3 Comparison between sensors***

In terms of overall accuracy IKONOS gave better results than Hyperion. The accuracy of Ikonos was higher than Hyperion when the raw images are compared. After deglinting, IKONOS results were higher by an even more significant margin. The radiometric resolution, sensor calibration, and the pixel size are some of the reasons for lower accuracy with Hyperion. The low signal to noise ratio in this sensor is an important element to be considered after the atmospheric correction. Low signal from the target of interest (i.e. seagrass, sand, or coral) adds error in the classification. The spectral mixing in one single pixel of Hyperion (30 meters) could be another source of error, because it can cover an extensive area of these relative small reefs and different bottom types could be produced different signals that are mixed in the same pixel. Using Hyperion the spectral mixing is very high. In contrast, IKONOS with a higher spatial resolution (1 meter) has lower spectral mixing of benthic features per pixel. This increases the accuracy of pixel classification. The mixing of components in the pixel classification is the basis for the accuracy when classifying benthic features.

## **Chapter 5**

### **DISCUSSION**

Benthic communities in shallow areas are mapped better. Sands and seagrass are well mapped in Cayo Enrique. Sea grasses and sands are located in the back reef lagoon which is a shallow region. The areas selected for testing sand were in the back reef lagoon and are mostly uniform sand areas. Carbonate sands and reef rubble in the reef crest are also well mapped. Sand areas along the study site are relatively shallow and mostly homogeneous as seen in IKONOS.

Seagrass had good accuracies in most image classifications. Coverage of sea grass areas is very uniform in the study site and therefore the training pixels were very homogeneous. Errors of commission occur for this class because other types of vegetation are classified as sea grass, like syringodium. Seagrass in the back reef lagoon is mostly homogeneous. Bottom with sand and seagrass were much better classified than corals. Corals are in deeper regions of the reef and are difficult for mapping due to the depths of wavelength penetration. Coral bottoms were misclassified as shallow areas and submarine vegetation, such as algae. The photosynthetic algae in the coral can be confused spectrally with seagrass or other type of vegetation. A relatively low accuracy was found when mapping corals in La Parguera.

The characteristics of the reef could be responsible for that because the specific area for testing the methods have corals at a slope of 45 degrees in the reef front and most of the corals in the area of study are sparse even when in the tested area the corals were very shallow (1 meter). The water column exerts a strong effect in the signal of coral communities, especially those in deeper areas where absorption and scattering in the

water column are higher. Detailed classification of corals (i.e. subclasses) or even percentage coral cover per area cannot be obtained with the tested methods. The classifications using the water column depth invariant index bands in IKONOS produced very low overall accuracy when compared with field data. Low accuracies are obtained after this processing because during this processing spectral information is lost. The results show that the classification after deglinting of IKONOS image and prior to water column correction resulted in the best overall accuracies for this sensor.

The best results obtained in the classifications performed with IKONOS and Hyperion images were the supervised Minimum Distance classifications. This was the supervised classification applied after all the processing methods.

Benthic habitats are in continuous change through the years. Another source of error in this study was the disparities in acquisition dates of the images and the field survey. Hyperion data were acquired in 2002 and IKONOS data in 2000. Field surveys were conducted between summer 2004 and 2005. The lack of metadata in IKONOS image required a dark pixel subtraction method (ENVI 4.0) for atmospheric correction instead of a more effective method for atmospheric correction. All these factors add inaccuracy to the results in the image classifications and are limitations in the comparison between sensors.

## **Chapter 6**

### **CONCLUSIONS**

Ikonos provides the best reference map for La Parguera region. According to the analyses and techniques used in this study the overall accuracy of IKONOS deglinted image was significantly higher than with Hyperion for mapping benthic habitats in La Parguera, Puerto Rico. These results show the benefits of higher spatial resolution when mapping benthic features. After deglinting, the IKONOS accuracies were higher by an even more significant margin. Ikonos shows good overall accuracy and kappa coefficient results. The results show that the classification after deglinting of IKONOS image and prior to water column correction is the best classification map for La Parguera.

In general good accuracies were obtained when mapping coral reefs at la Parguera. Hyperion raw data shows similar accuracy to Ikonos raw data when mapping coral reefs in La Parguera. It shows the importance of good spectral and spatial resolution. The radiometric resolution, sensor calibration, and the pixel size are some of the reasons for lower accuracy with Hyperion. The low signal to noise ratio in this sensor is an important element to be considered after the atmospheric correction. Hyperion spectral resolution is superior but the spatial resolution of this sensor is a limitation as a result of the mixing of components in each pixel. In a singular pixel of 30 meters various benthic habitats are included and the level of mixing is too high. The method for image classification of Hyperion image did not used spectral field data as a reference classification of the benthic habitats. This is a point to be considered in the resulting maps that were classified based in the transect GPS location of benthic habitats. The results in this research show that the

best accuracy was obtained with Ikonos sensor after deglinting. Accuracies of both sensors were very similar prior to the application of the algorithms for performance therefore the application of other methods could improve the Hyperion map accuracies. Ikonos has shown good overall accuracies although it has not been atmospherically corrected with an atmospheric correction module like ACORN. The good spatial resolution is definitely a characteristic that a sensor should have in order to study benthic habitats.

This research provides the baseline for future habitat studies at la Parguera and for the testing of other sensors in this region. Field data collected for this project has been already used by engineering students in the testing and development of new image processing techniques and algorithms. The data and results included in this research can assist in the selection of the appropriate techniques and sensors to study benthic habitats at la Parguera. In general these studies are a reference for engineers in the development of sensors, image processing techniques and algorithms and for scientists in the selection of cost effective, time effective sensors and processing techniques. This is another example of the need to develop a sensor with the qualifications to study underwater features.

## Chapter 7

### RECOMMENDATIONS

Based on our work we recommend a most intensive image processing of both sensors in order to improve the atmospheric and water column corrections. Bathymetric corrections should be included in the analyses to be conducted in order to compensate for variable depth. The Lyzenga method is an image based technique for bathymetric correction. Other methods of predicting bathymetry are; Benny and Dawson Method (1983), Jupp Depth of Penetration Zones Method (1988), and the Lyzenga method. Bathymetric maps, sonar data and airborne LIDAR data are just some examples of data that can be complementary to remote sensing studies. The optical properties of the water column should be considered in order to understand the signal received by the sensor. It is also important to consider the radiometric, spectral, and spatial resolutions of the sensors used for these purposes. Perhaps it will be necessary to test other remote sensors, like the recently improved AVIRIS. Sensors like AVIRIS, LASH and QuickBird are some examples of the systems developed for earth studies that can be tested in this area. Because Hyperion has low signal to noise ratio we have to test other spectroscopic sensors, such as AVIRIS in order to compare the benefits of high spatial resolution versus high spectral resolution.

In terms of image collection, the date of collection and the field work should be completed at the same time. Benthic habitats are in constant change in particular the movement of the sands in the reef. Field transects should include percentage of coral cover, sea grass or sand and the mixing of these components. Future field work should

include a quantification of the cover percent of the classes (sand, seagrass and coral). Field validation data and transect data should include more points for reference and points dispersed along the entire area of study and other reefs at La Parguera in order to reduce bias in the results .

## Chapter 8

### REFERENCES

- Acevedo R., Morelock J., Olivieri R.A. 1989. Modification of Coral Reef Zonation by Terrigenous Sediment Stress. *PALAIOS* , V. 4, p 92-100
- Andréfouët S., Kramer P., Torres Pulliza D., Joyce K.E., Hochberg E.J., Garza- Perez R., Mumby P.J., Riegl B., Yamano H., White W.H., Zubia M., Brock J.C., Phinn S.R., Naseer A., Hatcher B.G., Muller-Karger F.E. 2003. Multi-site evaluation of IKONOS data for classification of tropical coral reef environments. (Unpublished). *Remote Sensing of the Environment*.
- Boardman, J. W., Kruse, F. A., and Green, R. O., 1995, Mapping target signatures via partial unmixing of AVIRIS data: in *Summaries, Fifth JPL Airborne Earth Science Workshop, JPL Publication 95-1*, v. 1, p. 23-26.
- Clark R.N. , Swayze G.A., King T.V., Livo K.E., Kokaly R.F., Dalton J.B., Vance J.S., Rockwell B.W. and R.R. McDougal. Surface Reflectance Calibration of Terrestrial Imaging Spectroscopy Data: a Tutorial using AVIRIS. Denver Spectroscopy Laboratory, U.S. Geological Survey, Denver, Colorado.  
<http://speclab.cr.usgs.gov/PAPERS/calibration/tutorial/calibntA.html>
- Green E., Alasdair E., Clark C. and J. Mumby. 2000. Remote Sensing Handbook for Tropical Coastal Management. Unesco Publishing. Coastal management sourcebooks 3. Chapter 4 and 7.
- Green R.O., Eastwood M.L., Sarture C.H.M., Chrien T.G., Aronsson M., Chippendale B.J., Solis M., Olah M.R. and O. Williams. 1998. Imaging Spectroscopy and the

- Airborne Visible Infrared Imaging Spectrometer (AVIRIS). *Remote Sensing of the Environment* 65:227-248.
- Green, A. A., Berman, M., Switzer, B., and Craig, M. D., 1988, A transformation for ordering multispectral data in terms of image quality with implications for noise removal: *IEEE Transactions on Geoscience and Remote Sensing*, v. 26, no. 1, p. 65 - 74.
- Goodman, J.A., 2004. Hyperspectral Remote Sensing of Coral Reefs Deriving Bathymetry, Aquatic Optical Properties and a Benthic Spectral Unmixing Classification Using AVIRIS data in the Hawaiian islands. Ph.D. Dissertation.
- Goodman, J.A., Ustin, S.L., 2003, *Airborne Hyperspectral Analysis of Coral Ecosystems in the Hawaiian Islands*,. 30th International Symposium on Remote Sensing of Environment, Honolulu, Hawaii.
- Holden H. and E. Le Drew. 2001. Effects of the Water Column on Hyperspectral Reflectance of Submerged Coral Reef Features, *Bulletin of Marine Science*, 69 (2): 685- 699.
- Holden H. and E. Le Drew. 2001. Hyperspectral discrimination of healthy versus stressed corals using in situ reflectance. *Journal of Coastal Research* 17, 4;850-858
- Hochberg E. J. and Atkinson M.J., 2000. Spectral discrimination of coral reef benthic communities. *Coral Reefs*19;164-171
- Hochberg E. J., Andréfouët S., and Tyler M. R., “Sea Surface Correction of High Spatial Resolution IKONOS Images to Improve Bottom Mapping in Near-Shore Environments” *IEEE Transactions on Geoscience and Remote Sensing*, Vol. 41, NO. 7, July 2003

- Hochberg E. J., Atkinson M.J., Andréfouët S. 2003. Spectral reflectance of coral reef of bottom types worldwide and implications for coral reef remote sensing. *Remote Sensing of the Environment*.85; 159-173
- Hochberg E. J. and Atkinson M.J., 2003. Capabilities of remote sensors to classify coral, algae and sand as pure and mixed spectra. *Remote Sensing of the Environment*.85; 174-189
- Kendall M.S., Kruer D.R., Buja K.J., Christensen J.D., Finkbeiner M. and M.E.Monaco. 2002. NOAA National Oceanic and Atmospheric Administration, “ Methods used to map the benthic habitats of Puerto Rico and the U.S. Virgin Islands” , NOAA Technical Memorandum NOS NCCOS CCMA 152 . National Centers for Coastal Ocean Science, center for Coastal Monitoring and Assessment, Biogeography Team.
- Lee Z., Carder K.L., Chen R.F. and T. G. Peacock. 2001. Properties of the water column and bottom derived from Airborne Visible Infrared Imaging Spectrometer, AVIRIS, data, *Journal of Geophysical Research* , Vol. 106, No. C6, pages 11,639-11,651, June 15.
- Lyzenga D.R., 1981. Remote sensing of bottom reflectance and water attenuation parameters in shallow water using aircraft and Landsat data. *International Journal of Remote Sensing*, 2, 71-82
- Morelock J., Ramirez W.R., Bruckner A.W. and M. Carlo. 1994; 2000. Status of Coral Reefs Southwest Puerto Rico, *Caribbean Journal of science* vol 20.

- Morelock J., Winget E.A. and C. Goenaga. 1994. Geologic Maps of the Southwestern Puerto Rico Parguera to Guanica Insular Shelf, U.S. Department of the Interior, U.S.G.S. To accompany Map-I- 2387.
- Mueller J.L., Fargion G.S. and C.R. McClain. 2003. Ocean Optics Protocols for Satellite Ocean Color Sensor Validation, Revision 4, Volume IV: Inherent Optical Properties: Instruments, Characterizations, Field Measurements and Data Analysis Protocols cp 12.
- Mumby P.J. and Edwards A.J. 2002. *Mapping marine environments with IKONOS imagery: enhanced spatial resolution can deliver greater thematic accuracy.* Remote Sensing of the Environment 82(2002) 248-257
- Mumby P.J., Green E.P., Edwards A.J. and Clark C.D., 1997. Measurement of seagrass standing crop using satellite and digital airborne remote sensing. Marine Ecology Progress Series. Vol. 159; 51-60
- Mustard J.F, Staid M.I and Fripp W.J. 2001. A semi analytical approach to the calibration of AVIRIS data to reflectance over water application in a temperate estuary. Remote sensing of Environment. 75 (2001) 335-349
- Stumpf R.P. and K. Holderied. 2003. Determination of Water depth with high resolution satellite imagery over variable bottom types. Limnol. Oceanogr. 48 (I part 2), 547-556
- Toole D. A., Siegel D. A., Menzies D.W., Neumann M.J. and R.C. Smith. 2000. Remote Sensing Reflectance Determinations in the Coastal Ocean Environment: Impact of Instrumental Characteristics and Environmental Variability, APPLIED OPTICS, Vol. 39 No. 3, January 20.

- Kruse F.A. 2002. Comparison of AVIRIS and Hyperion for hyperspectral mineral mapping. 11<sup>th</sup> JPL Airborne Geoscience Workshop , 4-8 March 2002 , Pasadena California.
- Kruse F.A. 2003. Preliminary Results-Hyperspectral mapping of coral reef systems using EO-1 Hyperion, Buck Island, U.S. Virgin Islands. 12<sup>th</sup> JPL Airborne Geoscience Workshop, 24-28 February, 2003.
- Kruse F.A., Richardson L.L. and Ambrosia V.G., 1997. Fourth International Conference on Remote Sensing for Marine and Coastal Environments, Orlando, Florida 17-19 March 1997
- Kruse F. A. and Lefkoff A.B. 1993. "Knowledge-based geologic mapping with imaging spectrometers," *Remote Sens. Rev.*, vol. 8, pp. 3–28,.
- Kruse F. A., Boardman J. W., and Huntington J. F. 1999, "Fifteen years of hyperspectral data: Northern Grapevine Mountains, Nevada," in *Proc. 8th JPL Airborne Earth Science Workshop*, vol. 99–17. Pasadena, CA, 1999, pp. 247–258.
- Boardman J. W. and Kruse F. A., 1994 "Automated spectral analysis: A geologic example using AVIRIS data, North Grapevine Mountains, Nevada," in *Proce. 10th Thematic Conf. on Geologic Remote Sensing*, Ann Arbor, MI, 1994, pp. I-407–I-418.
- Kruse F. A., Boardman J.W., and Huntington J. F., "Comparison of airborne hyperspectral data and EO-1 hyperion for mineral mapping," 2003. *IEEE Transactions on geoscience and remote sensing*, vol. 41, No 6.

Green E., Alasdair E., Clark C. and J. Mumby .2000.Remote Sensing Handbook for Tropical Coastal Management. Unesco Publishing. Coastal management sourcebooks 3

Kruse F. A., Preliminary Results-Hyperspectral Mapping of Coral Reef Systems Using EO-1 HYPERION, Buck Island, USVI. 12th JPL Airborne Geoscience Workshop, 24-28 February 2003.

A.C.Rencher, 1995, Methods of multivariate analysis, New York: Wiley. pp.627

Richards J.A. and Jia Xiuping, 1999, Remote Sensing Digital Image Analysis, an introduction. Third edition. Springer Publishing. pp.189

Websites:

[http://geology.uprm.edu/Morelock/GEOLOCN\\_/INDEX.HTM](http://geology.uprm.edu/Morelock/GEOLOCN_/INDEX.HTM)

(Jack Morelock, site at University of Puerto Rico at Mayagüez)

<http://www.spaceimaging.com/>

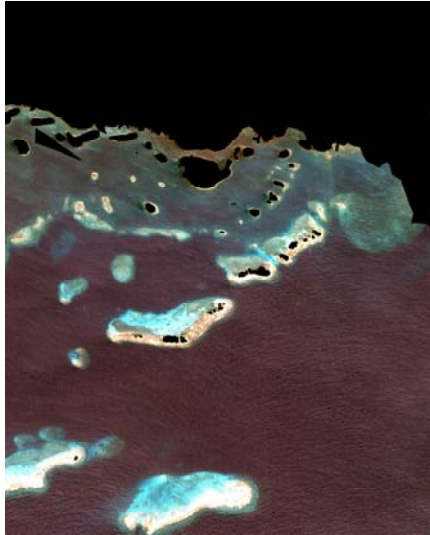
<http://geo.arc.nasa.gov/sge/landsat/17.html>

<http://eo1.gsfc.nasa.gov/Technology/Hyperion.html>

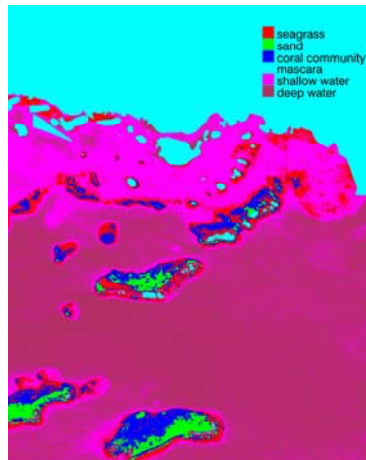
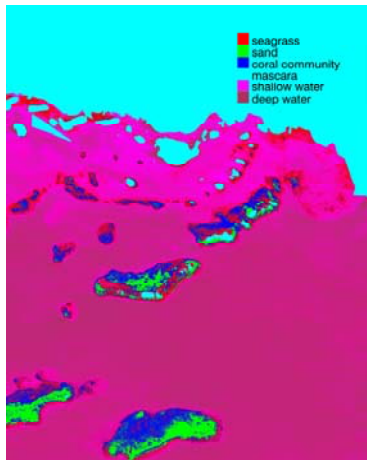
[http:// www.csc.noaa.gov/products/maine/html/casi.htm](http://www.csc.noaa.gov/products/maine/html/casi.htm)

## Appendix 1:

### Sun Glint correction for IKONOS image



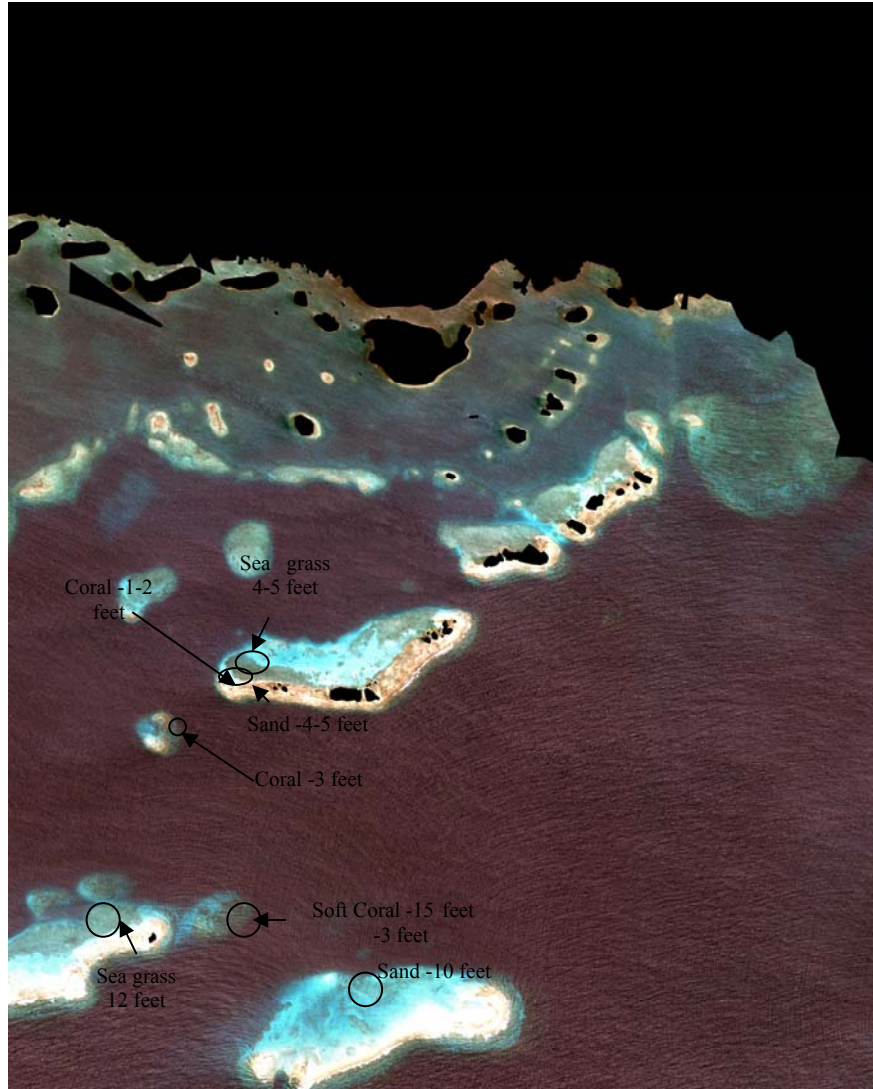
Left image shows Ikonos raw data with mask. Right image shows IKONOS deglinted image.



Minimum distance supervised classifications of IKONOS raw and Deglinted Image. Left, IKONOS raw image classification. Right, IKONOS deglinted image classification.

## Appendix 2:

### Water Column Correction –Lyzenga Method



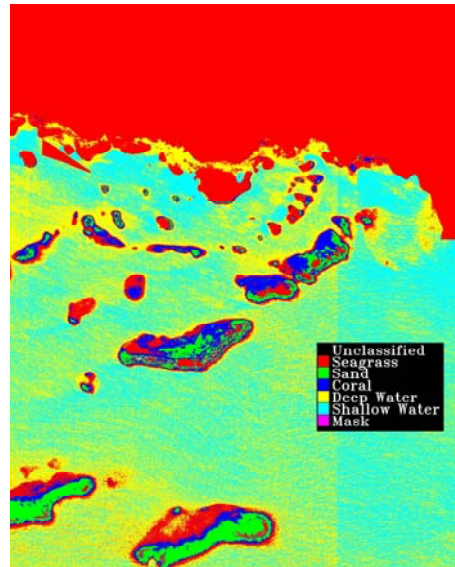
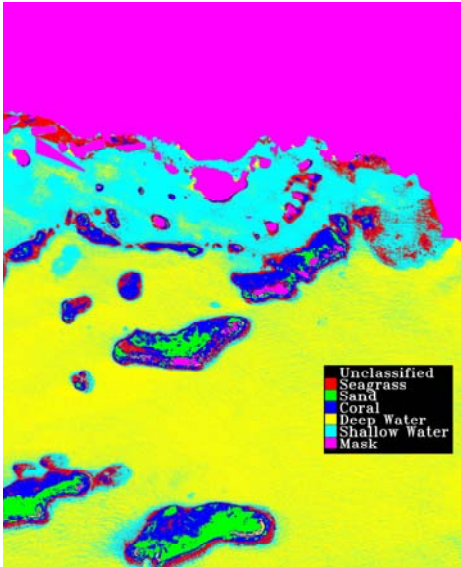
Regions selected from the digital imagery over areas of submerged sand, sea grass and coral for calculation of attenuation coefficients.

Table 1: Ratio of attenuation coefficient in band *I* and band *J* by substrate.

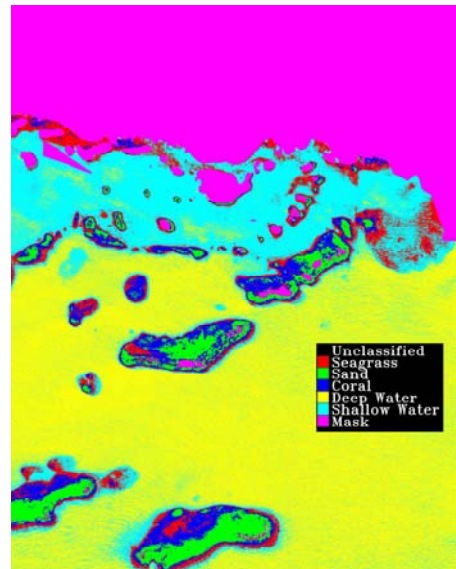
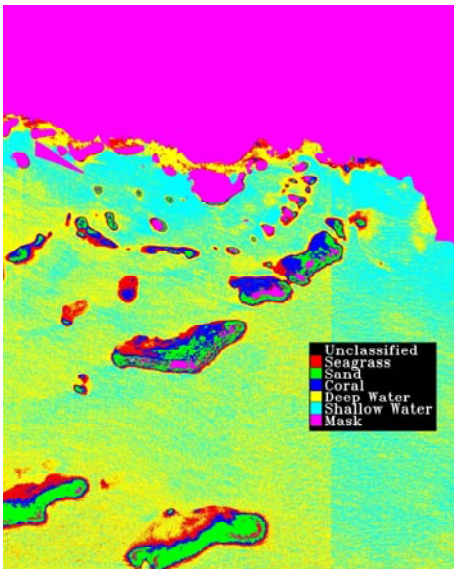
<b>Substrate</b>	<b>Ln Bands</b>	<b>(K<sub>i</sub>/K<sub>j</sub>)Ratio of attenuation coefficients in band i and band j</b>
<b>Sand</b>	<b>Red vs. Green</b>	<b>0.7703</b>
	<b>Green vs. Blue</b>	<b>0.7697</b>
	<b>Red vs. Blue</b>	<b>0.6016</b>
<b>Seagrass</b>	<b>Red vs. Green</b>	<b>0.7659</b>
	<b>Green vs. Blue</b>	<b>0.7248</b>
	<b>Red vs. Blue</b>	<b>0.5536</b>
<b>Coral</b>	<b>Red vs. Green</b>	<b>0.5661</b>
	<b>Green vs. Blue</b>	<b>0.6324</b>
	<b>Red vs. Blue</b>	<b>0.3818</b>

## Water Column Correction –Lyzena Method Depth Invariant Index Bands

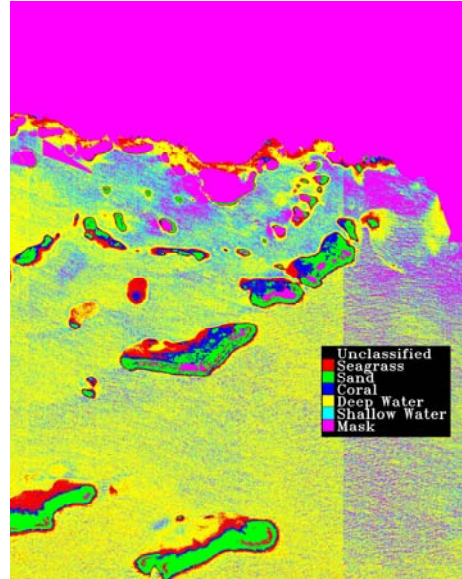
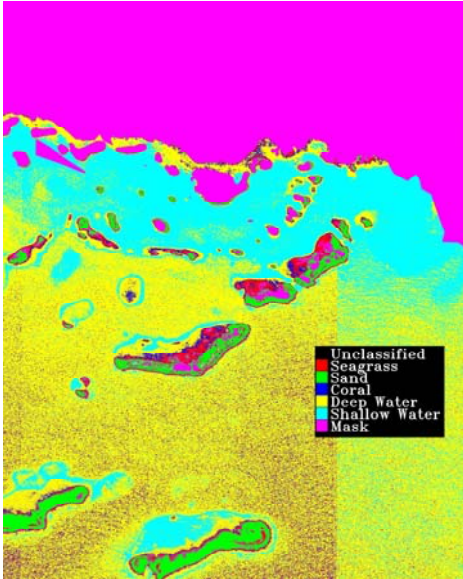
### Coral Depth Invariant Index Band



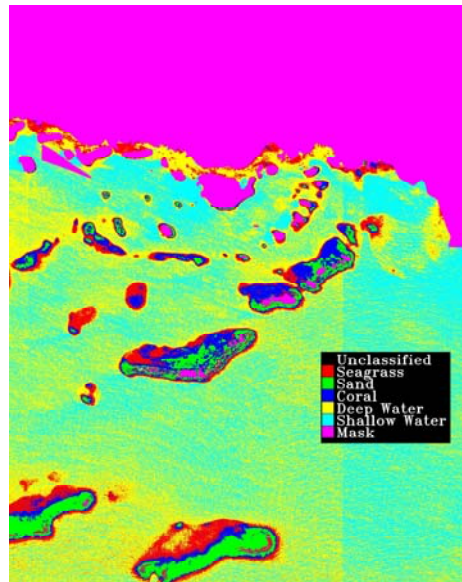
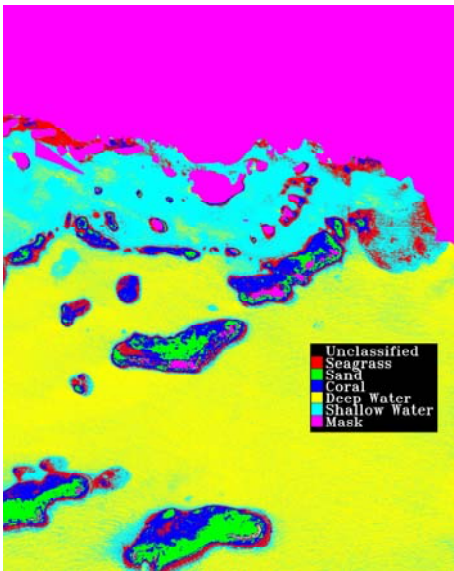
Left ,Coral Green vs Blue DII minimum distance classification.. Right, Red vs. Blue DII minimum distance classification.



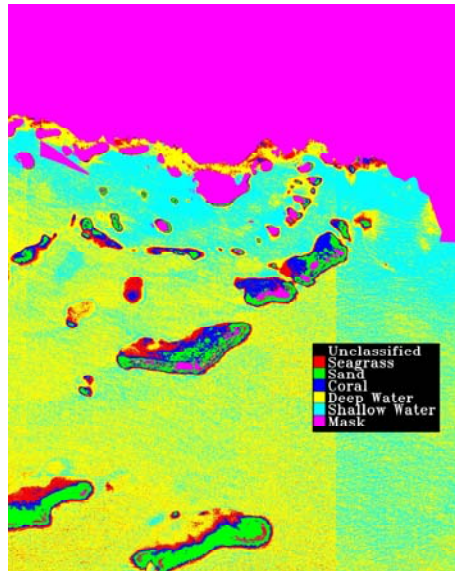
Left, Coral red vs green DII minimum distance classification. Sand green vs. Blue DII minimum distance classification.



Left ,sand red vs.green DII minimum distance classification. Right sand red vs. blue DII minimum distance classification.

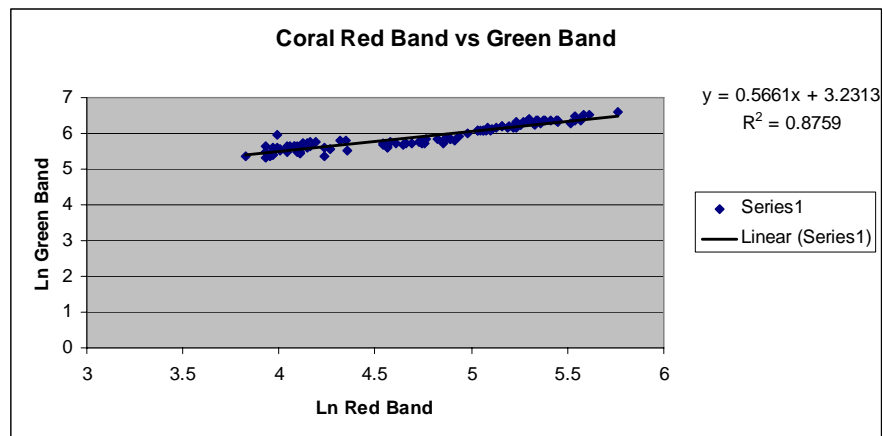


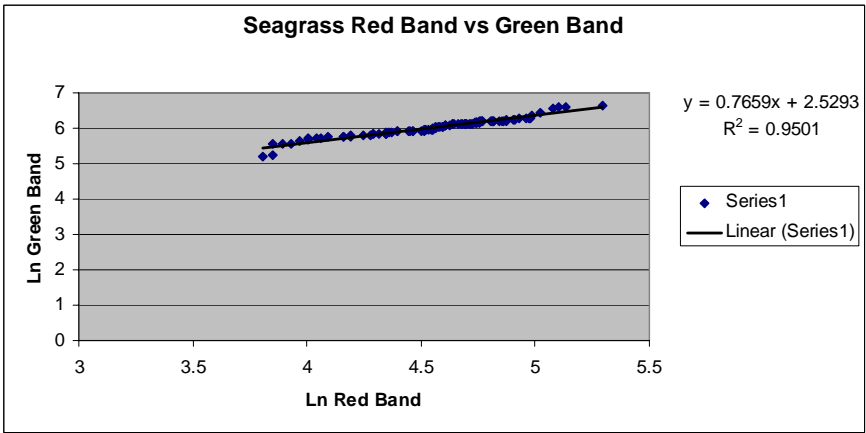
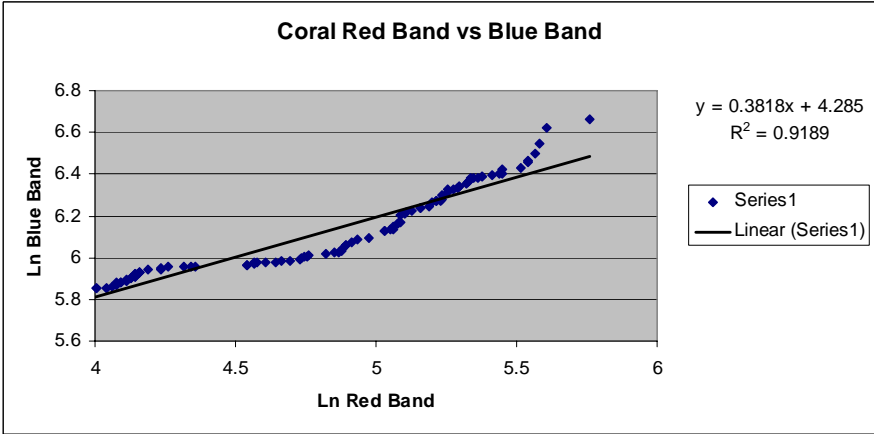
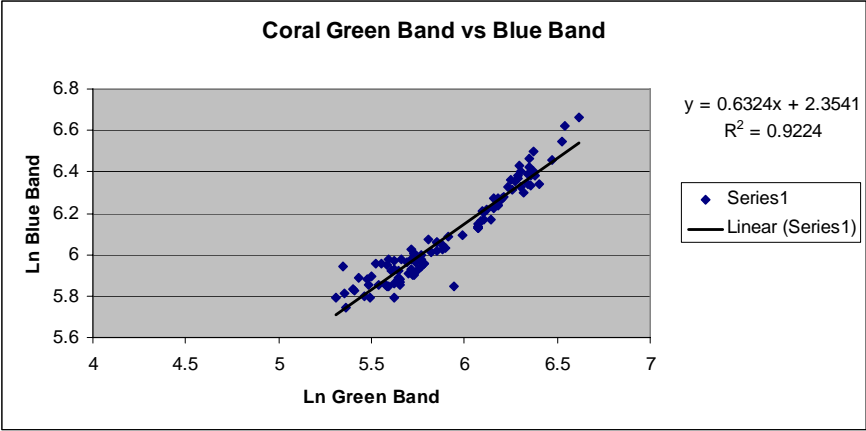
Left, seagrass green vs. blue DII minimum distance classification.seagrass red vs blue

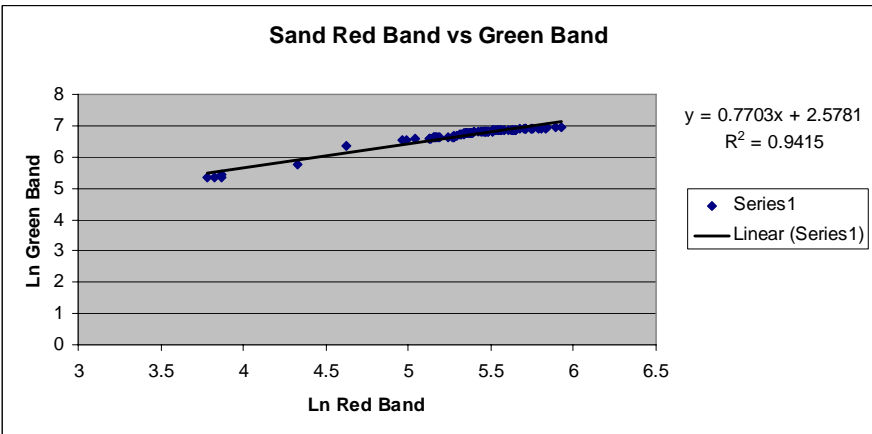
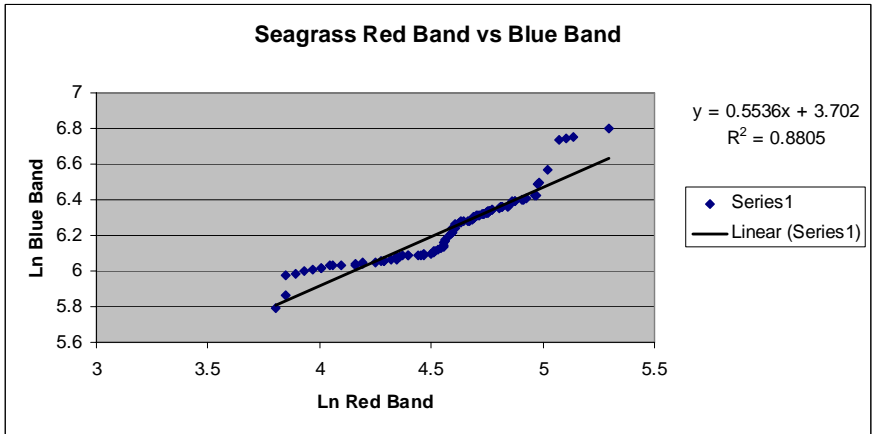
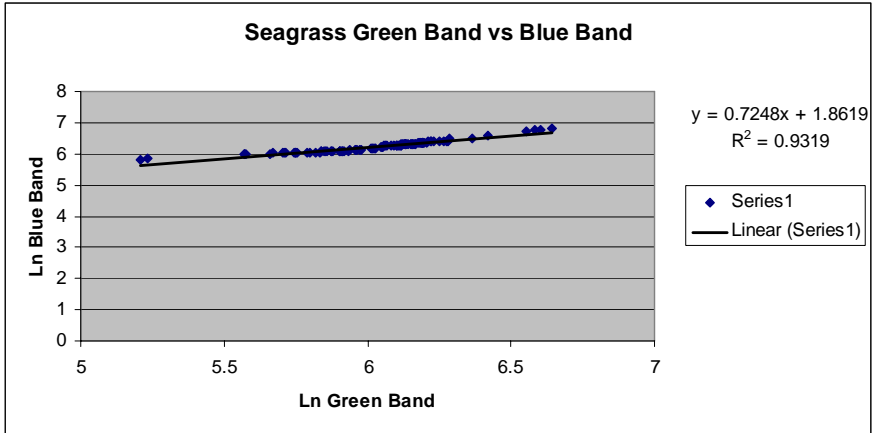


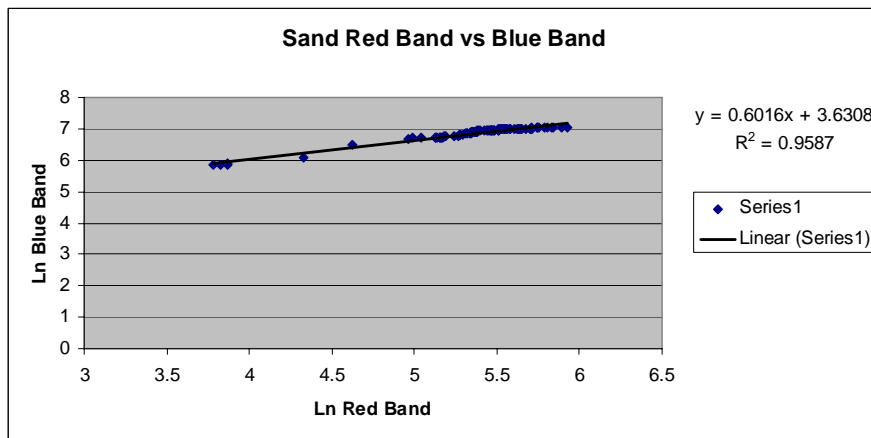
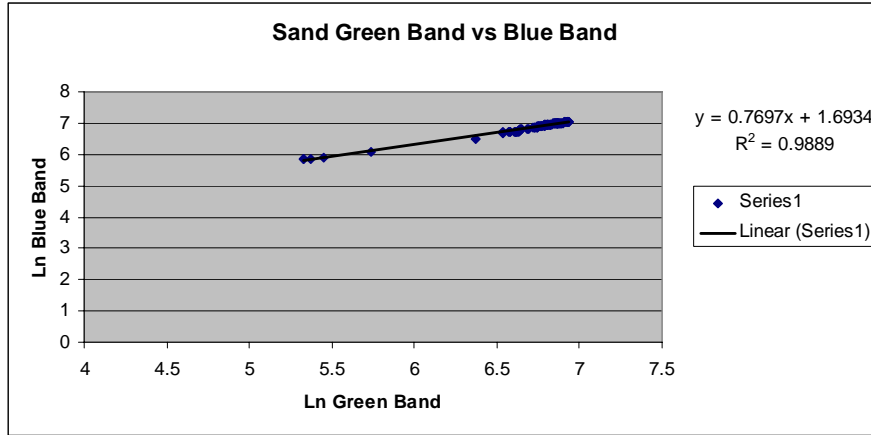
Sea grass red vs. green DII minimum distance classification.

**Lyzenga Method –water column correction. Depth invariant index biplot graphs.**





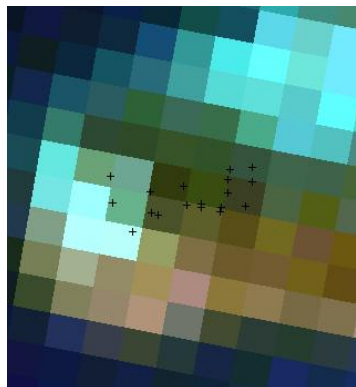
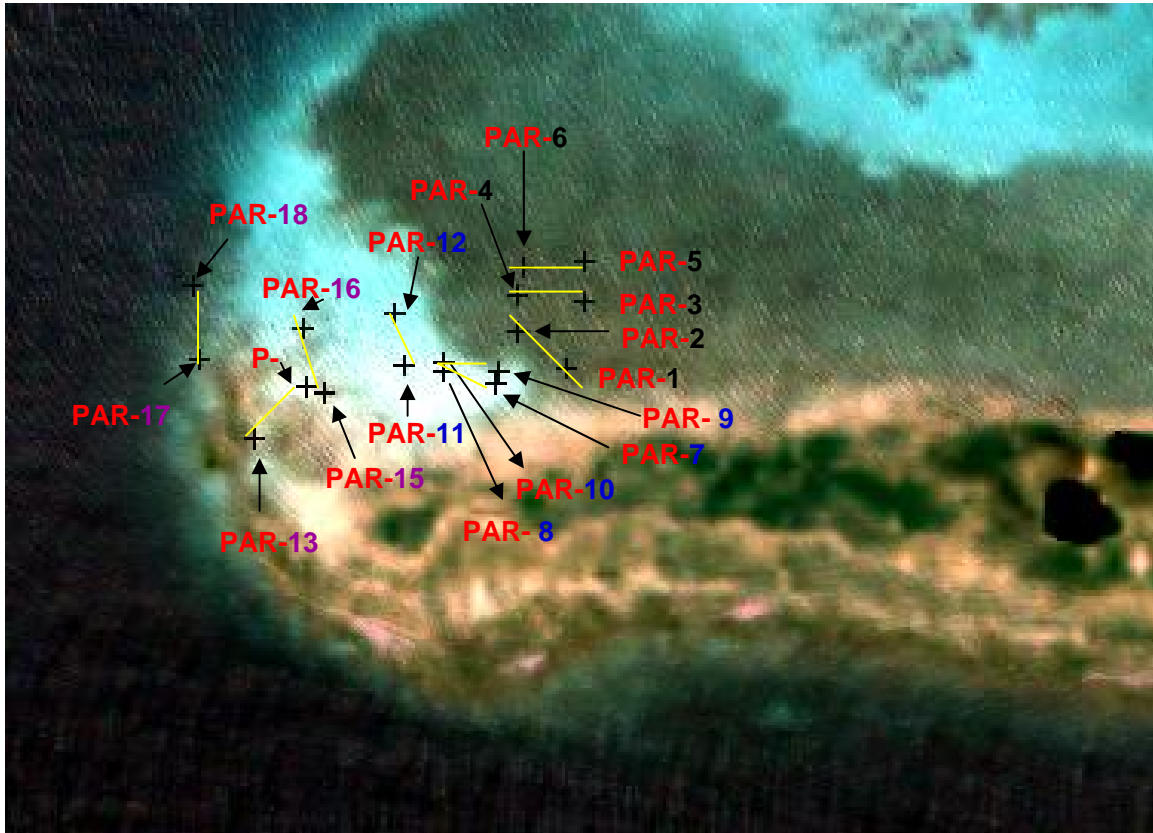




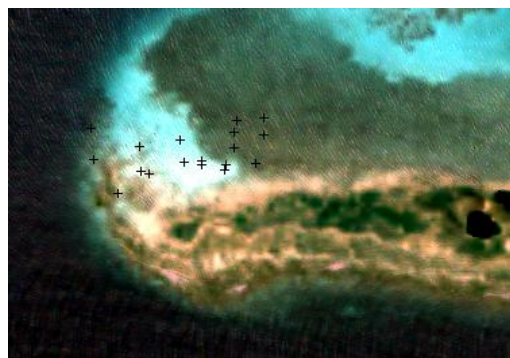
### Appendix 3:

#### Transect data points

Location of transect GPS data points: Seagrass- black, sand-blue, coral-purple. Yellow lines represent transect approximate location.



HYPERION GPS POINT



IKONOS GPS POINTS

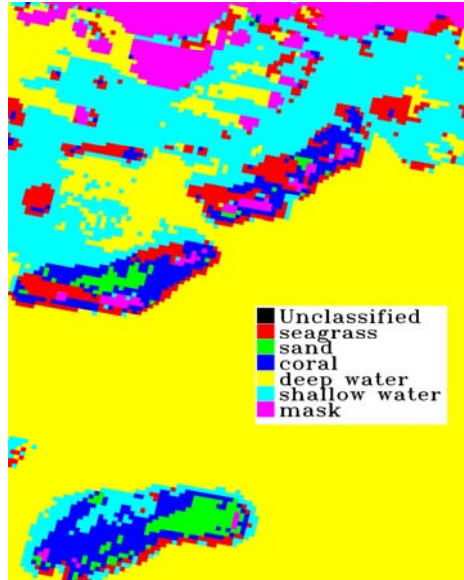
**GPS data point of transects**

<b>SUBSTRATE</b>	<b>TRANSECT</b>	<b>EAST POINT</b>	<b>WEST POINT</b>	<b>GPS Point</b>
<b>Seagrass</b>	1	East Point 17 <sup>0</sup> 57' .291 67 <sup>0</sup> 03' .122"	West Point 17 <sup>0</sup> 57' .297" 67 03' .131"	East -PAR-1  West-PAR2
	2	East Point 17 <sup>0</sup> 57' .303" 67 <sup>0</sup> 03' .118"	West Point 17 <sup>0</sup> 57' .304" 67 <sup>0</sup> 03' .131"	East -PAR-3  West-PAR-4
	3	East Point 17 <sup>0</sup> 57' .310" 67 <sup>0</sup> 03' .119"	West Point 17 <sup>0</sup> 57' .308" 67 <sup>0</sup> 03' .130"	East -PAR-5  West-PAR-6
<b>Sand</b>	1	East Point 17 <sup>0</sup> 57' .288" 67 <sup>0</sup> 03' .135"	West Point 17 <sup>0</sup> 57' .290" 67 <sup>0</sup> 03' .144"	East -PAR-7  West-PAR-8
	2	East Point 17 <sup>0</sup> 57' .290" 67 <sup>0</sup> 03' .134"	West Point 17 <sup>0</sup> 57' .292" 67 <sup>0</sup> 03' .144"	East -PAR-9  West-PAR-10
	3	<b>South Point</b> 17 <sup>0</sup> 57' .291" 67 <sup>0</sup> 03' .152"	<b>North Point</b> 17 <sup>0</sup> 57' .301" 67 <sup>0</sup> 03' .154"	South- PAR-11  North- PAR-12
<b>Coral</b>	1	<b>South Point</b> 17 <sup>0</sup> 57' .278 67 <sup>0</sup> 03' .179	<b>North Point</b> 17 <sup>0</sup> 57' .287 67 <sup>0</sup> 03' .170	South- PAR-13  North- PAR-14
	2	<b>South Point</b> 17 <sup>0</sup> 57' .286 67 <sup>0</sup> 03' .167	<b>North Point</b> 17 <sup>0</sup> 57' .298 67 <sup>0</sup> 03' .171	South- PAR-15  North- PAR-16
	3	<b>South Point</b> 17 <sup>0</sup> 57' .298 67 <sup>0</sup> 03' .171	<b>North Point</b> 17 <sup>0</sup> 57' .292 67 <sup>0</sup> 03' .190	South- PAR-17  North- PAR-18

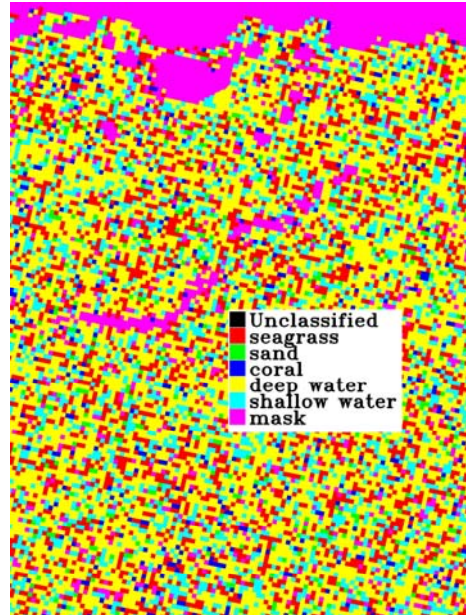
### GPS Points in the image

GPS Point	Coordinates
PAR-1-	17 <sup>0</sup> 57' 17.45" N 67 <sup>0</sup> 3' 7.31" W
PAR-2	17 <sup>0</sup> 57' 17.84 N 67 <sup>0</sup> 3' 7.85 W
PAR-3	17 <sup>0</sup> 57' 18.17 N 67 <sup>0</sup> 3' 7.11 W
PAR-4	17 <sup>0</sup> 57' 18.23 N 67 <sup>0</sup> 3' 7.85 W
PAR-5	17 <sup>0</sup> 57' 18.59 N 67 <sup>0</sup> 3' 7.11 W
PAR-6	17 <sup>0</sup> 57' 18.52 N 67 <sup>0</sup> 3' 7.79 W
PAR-7	17 <sup>0</sup> 57' 17.29 N 67 <sup>0</sup> 3' 8.06 W
PAR-8	17 <sup>0</sup> 57' 17.41 N 67 <sup>0</sup> 3' 8.67 W
PAR-9	17 <sup>0</sup> 57' 17.42 N 67 <sup>0</sup> 3' 8.06 W
PAR-10	17 <sup>0</sup> 57' 17.51 N 67 <sup>0</sup> 3' 8.67 W
PAR-11	17 <sup>0</sup> 57' 17.48 N 67 <sup>0</sup> 3' 9.11 W
PAR-12	17 <sup>0</sup> 57' 18.03 N 67 <sup>0</sup> 3' 9.21 W
PAR-13	17 <sup>0</sup> 57' 16.69 N 67 <sup>0</sup> 3' 10.77 W
PAR-14	17 <sup>0</sup> 57' 17.25 N 67 <sup>0</sup> 3' 10.20 W
PAR-15	17 <sup>0</sup> 57' 17.18 N 67 <sup>0</sup> 3' 9.99 W
PAR-16	17 <sup>0</sup> 57' 17.86 N 67 <sup>0</sup> 3' 10.23 W
PAR-17	17 <sup>0</sup> 57' 17.54 N 67 <sup>0</sup> 3' 11.39 W
PAR-18	17 <sup>0</sup> 57' 18.32 N 67 <sup>0</sup> 3' 11.46 W

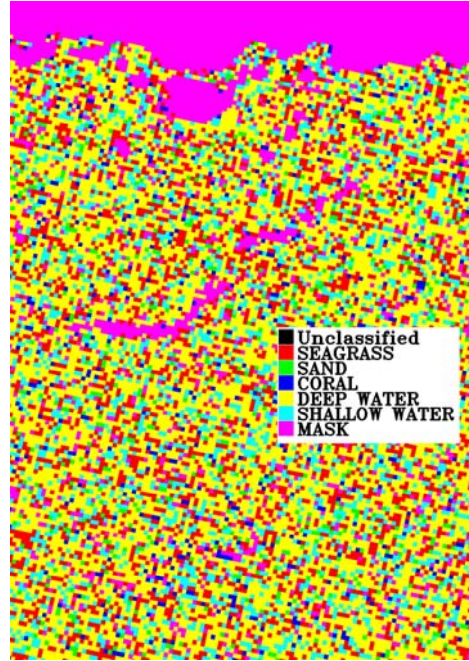
**Appendix 4:  
Hyperion classifications**



Hyperion Envi raw image (Left), Minimum distance classified image (Right).



Hyperion atmospheric corrected and destriped image (Left), minimum distance classified image (Right).



Hyperion atmospheric corrected, destriped and deglinted image (Left), minimum distance classified image (Right).